

SOIL WATER HYSTERESIS IN THE  
INTER-AGGREGATE VOIDS OF TWO  
HAWAIIAN OXISOLS

A THESIS SUBMITTED TO THE GRADUATE DIVISION OF THE  
UNIVERSITY OF HAWAII IN PARTIAL FULFILLMENT  
OF THE REQUIREMENTS FOR THE DEGREE OF

MASTER OF SCIENCE

IN AGRONOMY AND SOIL SCIENCE

MAY 1974

By

Lance T. Santo

Thesis Committee:

Richard E. Green, Chairman  
James A. Silva  
Gordon Y. Tsuji  
Goro Uehara

## TABLE OF CONTENTS

	Page
LIST OF TABLES . . . . .	v
LIST OF FIGURES . . . . .	vi
INTRODUCTION . . . . .	1
REVIEW OF LITERATURE . . . . .	3
Soil-Water Hysteresis . . . . .	3
Mathematical Simulation of Hysteresis . . . . .	4
MATERIALS AND METHODS . . . . .	7
Soils . . . . .	7
Soil Column . . . . .	8
Packing of Soil Column . . . . .	10
Flow System . . . . .	10
Pressure Measurements . . . . .	12
Water Content Measurements . . . . .	13
Hysteretic Measurements . . . . .	13
RESULTS AND DISCUSSION . . . . .	17
Experimental Hysteresis Data . . . . .	17
Experimental versus Calculated . . . . .	22
Parameter Relationships . . . . .	30
Absorption Curves . . . . .	31
Desorption Curves . . . . .	31
Predicted Scanning Curves for the Molokai Soil . . . . .	37
Calculated Hydraulic Conductivity . . . . .	42
IMPLICATION OF RESULTS AND SUMMARY . . . . .	46
LITERATURE CITED . . . . .	48

## TABLE OF CONTENTS, CONTINUED

	Page
APPENDIX A . . . . .	52
APPENDIX B . . . . .	74
APPENDIX C . . . . .	79
APPENDIX D . . . . .	82
APPENDIX E . . . . .	84
APPENDIX F . . . . .	92

## LIST OF TABLES

Table		Page
1	Aggregate Stability Analysis of the Molokai and Wahiawa Soils in the less than 2 mm Fraction. . . . .	9
2	Bulk Density and Water Content Measurements of the Molokai Soil with and without Resolving Time Correction. . . . .	69
3	Tabulation of the Molokai Soil Experimental Hysteresis Data. . . . .	75
4	Tabulation of the Wahiawa Soil Experimental Hysteresis Data. . . . .	77
5	Curve Fitting Parameters. . . . .	80
6	Interpolated Curve Fitting Parameters from Figures 19 and 20. . . . .	83

## LIST OF FIGURES

Figure		Page
1	Water Flow System. . . . .	11
2	Water Absorption Curves of the Molokai Soil. .	18
3	Water Desorption Curves of the Molokai Soil. .	19
4	Water Absorption Curves of the Wahiawa Soil. .	20
5	Water Desorption Curves of the Wahiawa Soil. .	21
6	Calculated and Experimental Absorption Curves of the Molokai Soil. . . . .	23
7	Calculated and Experimental Desorption Curves of the Molokai Soil. . . . .	24
8	Calculated and Experimental Absorption Curves of the Wahiawa Soil. . . . .	25
9	Calculated and Experimental Desorption Curves of the Wahiawa Soil. . . . .	26
10	Calculated and Experimental Absorption Curves of the Sandy Loam Soil (Topp's Data) . . . . .	27
11	Calculated and Experimental Desorption Curves of the Sandy Loam Soil (Topp's Data) . . . . .	28
12	Absorption Fitting Parameters ( $\theta_r$ versus $\beta$ or $\phi_0$ ) of the Molokai Soil. . . . .	32
13	Absorption Fitting Parameters ( $\theta_r$ versus $\beta$ or $\phi_0$ ) of the Wahiawa Soil. . . . .	33
14	Absorption Fitting Parameters ( $\theta_r$ versus $\beta$ or $\phi_0$ ) of the Sandy Loam Soil . . . . .	34

## LIST OF FIGURES, CONTINUED

Figure		Page
15	Desorption Fitting Parameters ( $\theta_0$ versus $\beta$ or $\phi_0$ ) of the Molokai Soil. . . . .	35
16	Desorption Fitting Parameters ( $\theta_0$ versus $\beta$ or $\phi_0$ ) of the Wahiawa Soil. . . . .	36
17	Desorption Fitting Parameters ( $\theta_0$ versus $\beta$ or $\phi_0$ ) of the Sandy Loam Soil . . . . .	38
18	Family of Predicted Absorption Scanning Curves for the Molokai Soil . . . . .	39
19	Family of Predicted Desorption Scanning Curves for the Molokai Soil . . . . .	40
20	Calculated Molokai Absorption and Desorption $K(\theta)$ Relationships . . . . .	43
21	Calculated Wahiawa Absorption and Desorption $K(\theta)$ Relationships . . . . .	44
22	Diagram of Gamma-ray Assembly and Instrumentation. . . . .	61
23	Experimental Verification of the Gamma-ray Attenuation Equation, with Water Thickness as the Independent Variable . . . . .	66
24	Experimental Verification of the Gamma-ray Attenuation Equation for Molokai Soil, with Mean Bulk Density as the Independent Variable.	68

## INTRODUCTION

In a porous media such as soil, water content changes in a cyclic nature. That is, in some regions of the soil, water is absorbed while at other locations it is being desorbed. In such a hysteretic flow system, the water content at a corresponding suction or pressure head depends upon previous absorption and desorption cycles. As a result no unique relationship exists between water content and pressure head. To complicate matters still further, an infinite number of desorption and absorption scanning curves are possible.

In the past, the effect of hysteresis on soil moisture redistribution was avoided by considering the system as either entirely absorbing or desorbing water. To simulate natural conditions, this phenomenon was incorporated into the unsaturated soil-water flow model (Bresler et al., 1969; Hanks et al., 1969; Staple, 1970). If hysteresis effects result in large differences in water contents, then the revised flow equation should give improved results.

Past studies by Sharma and Uehara (1968) have shown the existence of hysteresis in two highly aggregated Oxisols (Molokai and Wahiawa soils). These soils are texturally clay, but their water retention characteristics are similar to that of graded sand at low suctions. The present study is a more detailed analysis of the hysteretic nature of water in these two Oxisols. Hysteretic data are required for accurate prediction of the movement of water from mathematical models.

The objectives set forth are as follows:

- (1) To measure the hysteretic relationship between water content and suction in the inter-aggregate void spaces for

both Molokai and Wahiawa soils.

- (2) To test the modified equation (Gillham, 1973) of King (1965) to describe and predict the hysteretic behavior of water in both Oxisols.

## REVIEW OF LITERATURE

### Soil-Water Hysteresis

The existence of soil-water hysteresis has been well documented by earlier studies of Haines (1930), Smith et al. (1931) and Richard (1938). Basic analyses of this phenomenon in porous media were conducted by Miller and Miller (1956), Collis-George (1955), Young (1960), Staple (1969, 1970), Poulouvassilis (1969, 1970), Philip (1964), Topp and Miller (1966), Bomba (1968), Sharma and Uehara (1968), Talsma (1970), Topp (1969, 1971a, 1971b) and Smiles et al. (1971).

Three generally accepted postulates causing soil-water hysteresis are as follows:

1. The so-called "blocked pore" or "ink-bottle effect" due to the geometric nonuniformity of the individual pores.
2. Contact angle differences between water and soil during the absorption and desorption processes.
3. The effect of soil-water film thickness on the formation of a "hemispherical" meniscus at the "opening" of a pore.

Of the three, postulate (1) is considered to be more prevalent (Collis-George, 1955). Consequently, hysteresis would be expected to be much more pronounced in coarse-textured (Hillel, 1971) and in aggregated (Sharma and Uehara, 1968) soils than in fine textured soils.

Soil-water hysteresis is further complicated by the influences of entrapped air, temperature, biological activity, solute concentration and swelling, shrinking or aging phenomenon. Any changes in the physical and chemical properties of the soil-water system may have a significant effect on the magnitude of soil-water hysteresis. Complete discussions

of the aforementioned causes and factors affecting hysteresis have been presented by Topp (1964) and Davidson (1965).

#### Mathematical Simulation of Hysteresis

Earlier attempts to mathematically describe hysteresis has been limited to the application and testing of the independent domain theory formulated separately by Everett (1955) and Enderby (1955). The hypothesis enabled absorption and desorption scanning curves to be determined from absorption or desorption curves. The latter was obtained by adopting an arbitrary but plausible form of the normalized distribution density function. Good agreement between predicted and measured data was found for a glass bead medium (Poulovassilis, 1962) and for sand (Talsma, 1970; Poulovassilis, 1970). In contrast, however, studies by Morrow and Harris (1965), Topp and Miller (1966), Bomba and Miller (1967), Topp (1969, 1971a) and Vachaud and Thony (1971) have shown that the model was inadequate for media ranging from glass beads to clay loam soil.

The independent domain theory of hysteresis depended on the assumption that pore space can be divided into discrete volumes each of which drains and fills independently of the state of other pores. In the real situation, soil pores are usually inter-connected by a network of other pores, and the behavior of one pore is dependent on the state of the neighboring pores. Such pore interaction was suggested as the reason for the failure of the theory to describe hysteresis accurately in porous media. Everett (1967) extended the independent domain theory to allow one type of pore interaction to occur, and Topp (1971b) made allowances for two types of pore interactions. Both researchers found

improvements by accounting for interactions, but the model could not adequately predict hysteresis precisely over the suction range of their data.

An alternative model, proposed by King (1965) and subsequently modified by Gillham (1973), described hysteresis with a single function and provided the possibility of predicting hysteresis scanning curves from existing water characteristic data. No physical mechanism or interaction was assumed or suggested by this model. The model is principally a curve fitting process based on the primary scan and at least one secondary experimental hysteretic scan. Both King and Gillham reported excellent results with water content errors of less than 2% between the experimental and calculated results. Gillham was able to predict a family of absorption and desorption scanning curves between the main scans.

The mathematical model in the dimensionless form is expressed as

$$\theta = \theta_0 \frac{\cosh[(\phi/\phi_0)^\beta + \epsilon] - (\cosh\epsilon)(\theta_0 - \theta_r)/(\theta_0 + \theta_r)}{\cosh[(\phi/\phi_0)^\beta + \epsilon] + (\cosh\epsilon)(\theta_0 - \theta_r)/(\theta_0 + \theta_r)} \quad (1)$$

where  $\theta$  is the degree of saturation,  $\phi$  the dimensionless pressure head (pressure head divided by the soil column length), and  $\theta_0$ ,  $\theta_r$ ,  $\phi_0$ ,  $\beta$  and  $\epsilon$  are curve fitting parameters. Parameters  $\theta_0$  and  $\theta_r$  can be approximated at the limits imposed on equation (1). In the limit as  $\phi$  approaches zero,  $\theta$  approaches  $\theta_0$ , the degree of saturation at zero suction, and as  $\phi$  approaches negative infinity,  $\theta$  approaches  $\theta_r$ , the residual degree of saturation. The degree of saturation at zero suction cannot be explicitly determined, but only approximated since the function is discontinuous at  $\phi = 0$ . Three unknowns  $\phi_0$ ,  $\beta$  and  $\epsilon$  need to be determined. The boundaries of the unknowns are  $\phi_0 < 0$ ,  $\beta < 0$  and  $\epsilon > 0$ . These three parameters

determine the general curvature of the hysteretic function.

## MATERIALS AND METHODS

The characteristic hysteretic water content-suction relationships were determined for two Oxisols. A cylindrical plexiglas container or permeameter was packed with air-dried soil of less than 2 mm diameter. Uniformity of packing was determined by comparing the bulk densities, measured by gamma-ray attenuation, along the length of the permeameter. Thereafter, degassed water, with 0.1% phenol, was introduced into the soil system. Hysteretic main and scanning curves in the range of 0 to 200 cm of suction were determined under isothermal conditions ( $22 \pm 0.5^\circ$  C). Suction was measured by either elevation differences or applied vacuum. Water content determinations were obtained from gamma-ray attenuation methods.

A mathematical equation based on permeability studies of Gardner (1958) and King (1965) was employed as a means of storing large amounts of hysteresis data in the computer in a simple and useable form. Gillham (1973) modified the equation proposed by King and was able to predict scanning curves along the main curves from both primary and secondary scanning data.

### Soils

Two Oxisols classified as a Typic Torrox (Molokai) and a Tropeptic Eustrtox (Wahiawa) were used in the experiment. Both of these soils were collected on the island of Oahu. Selection of these soils was based on: (a) their agricultural importance in the cultivation of pineapple and sugarcane, (b) their use in previously related hysteresis studies, and (c) their similar mineralogical and chemical properties,

but different micromorphological properties (Tsuji, et al., 1974). Both soils are characterized by their high aggregate stability (Sharma and Uehara, 1968). The degree of aggregation and stability is greater in the Wahiawa soil (Cagauan and Uehara, 1965; Uehara et al., 1962). Table 1 represents the experimentally determined aggregate stability analysis for the <2 mm diameter fraction of the Molokai and Wahiawa soils by the wet-sieving method.

Air-dried soils (30-60 cm depth) which were passed through a 2 mm sieve were used in this study. For both Oxisols, packing of the <2 mm sieved soil material in the permeameter to a given bulk density results in a column of soil most nearly representative of the field situation (Southard, 1974).

#### Soil Column

The soil permeameter was fabricated out of a plexiglas cylinder having an inside diameter of 8.19 cm, 0.7 cm thick wall and vertical length of 20 cm. The top and base of a Tempe pressure cell<sup>1</sup> unit were used to enclose both ends of the cylinder. A fritted glass plate, with an experimentally determined air-entry value of 230 cm of water, was cemented to the base of the Tempe cell with silicone sealant<sup>2</sup>. In addition to the O-ring seated in the Tempe cell base, a rubber gasket was placed on the outer perimeter of the plate to ensure a water tight seal.

---

<sup>1</sup>Soil-Moisture Equipment Company of Santa Barbara, California, cat. no. 1400.

<sup>2</sup>General Electric Silicone Seal, Silicone Products Department, Waterford, New York.

TABLE 1

Aggregate Stability Analysis of  
Molokai and Wahiawa Soils in  
<2 mm Fraction

Diameter (mm)	% Oversize	
	<u>Molokai</u>	<u>Wahiawa</u>
.84	16.2	21.8
.42	43.7	55.7
.25	58.9	71.8
.10	77.9	85.1
<.10	100.0	100.0
log mean diameter (mm)	0.31	0.45

A second outlet was constructed at the base to permit removal of entrapped air, if any, under the porous plate.

### Packing of Soil Column

To eliminate higher bulk densities due to compaction at each end, plexiglas extension cylinders were taped to the top and the bottom of the soil column before loading the permeameter with soil. Air-dried soil was loaded through a funnel connected to a 120 cm long tube of 3.5 cm diameter. After the permeameter and extensions were filled, a 200 g weight was placed on top of the soil at the open top end before vibrating the column with a modified hand engraver. The average bulk density was calculated from the soil weight and permeameter volume. After securing the Tempe cell base to the soil column, the entire unit was placed on the gamma-ray column holder. The uniformity of soil packing was determined by comparing the bulk density at 1 cm intervals along the length of the column.

### Flow System

Water flowing into and out of the confined soil system could be controlled and measured through the flow system diagrammed in Figure 1. The air-dried soil was initially saturated by capillarity with water supplied from a Mariotte water reservoir, labeled reservoir (1). A graduated 25 ml buret was used in combination with reservoir (1) to obtain precise volume inflow and outflow measurements. After the soil was saturated, valve (1) at the base of reservoir (1) was closed. Thereafter, the volume of both inflow and outflow were measured by two inter-connected 25 ml and 250 ml burets, labeled as reservoir (2).

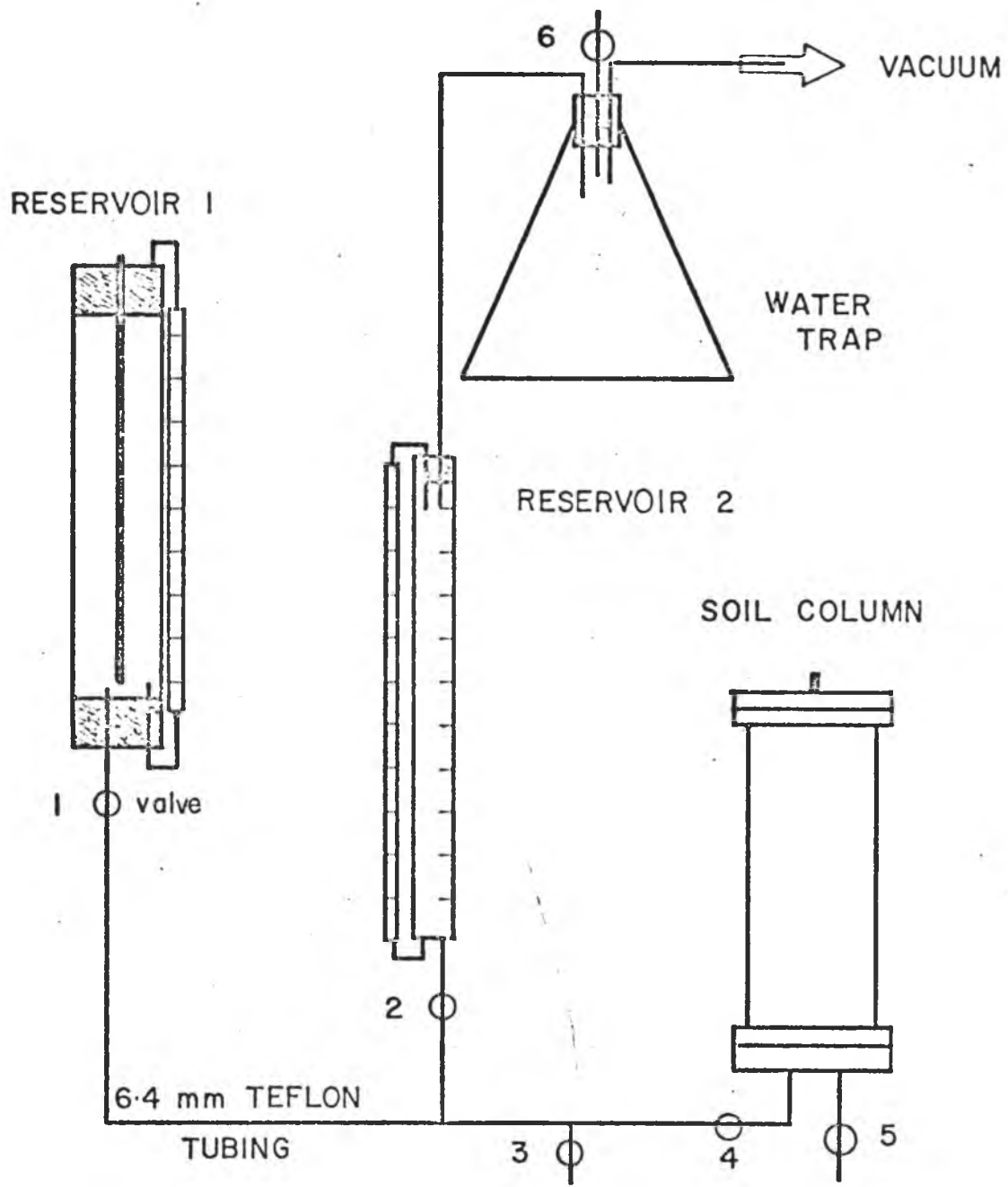


Figure 1. Water Flow System.

### Pressure Measurements

Suction was imposed on the system either by elevation difference or by vacuum. The former was determined by the hydraulic head difference between reservoir (2) and any given position of the stationary soil column which is described by the equation

$$h = -(z + L) \dots \dots \dots (2)$$

where  $h$  is the hydraulic head, or, in this case the pressure or suction head,  $z$  is the elevation difference measured in the upward direction, and  $L$  is any position along the length of the soil column. A vacuum pump<sup>3</sup> provided an alternative means of imposing suction. Vacuum was regulated with a Cartesian manostat<sup>4</sup>, and suction was determined by the difference between mercury levels in a U-tube manometer. Equation (2) is applicable here by substituting the negative pressure value for  $z$ . Both hydraulic head and mercury height differences were measured with a cathetometer<sup>5</sup>.

Times ranging from 10 to 48 hours were required for hydraulic equilibrium which was assumed to be established when there were no detectable changes in both the volume of water in reservoir (2) and the water content at each position.

---

<sup>3</sup>Duo Seal Vacuum Pump, model 1405, Welch Scientific Company, Skokie, Illinois.

<sup>4</sup>Cartesian Manostat, model no. 6a, cat. no. 50-570-00, Manostat Corp., 20 North Moore Street, New York, New York.

<sup>5</sup>Gaertner m-911 Cathetometer, Gaertner Scientific Corp., 1201 Wrightwood Avenue, Chicago, Illinois, 60614.

### Water Content Measurements

Rapid and non-destructive water content measurements were made by gamma-ray attenuation methods. A complete discussion of the gamma-ray unit is discussed in Appendix A. The basic attenuation equation used was

$$I = I_0 \exp(-\mu_c \rho_c x_c - \mu_s \rho_s x_s - \mu_w \rho_w x_w \theta) \dots (3)$$

where subscripts c, s and w refer to the empty column, soil and water, respectively, I the attenuated intensity,  $I_0$  the intensity at the gamma-ray source,  $\mu$  the mass attenuation coefficient of the attenuating material,  $\rho$  the density of the material, x its thickness and  $\theta$  the volumetric soil-water content.

The mass attenuation coefficients of water and the two soils were determined experimentally. Using these values, volumetric water content values were calculated from gamma-ray attenuation data. Water content measurements were made at 1 cm intervals length of the soil column.

### Hysteretic Measurements

After packing the permeameter with air-dried soil and measuring the gamma-ray intensities over the entire length of the permeameter at 1 cm intervals, the soil was gradually saturated with water by capillarity.

By adjusting the imposed vacuum, the soil-water content versus suction relationship could be experimentally determined for either the desorption or the absorption phase. After the initial draining, the main absorption and desorption curves were traced over the suction range of 0 to 200 cm of water. Sharma and Uehara (1968) indicated that the influence of the inter-aggregate void spaces for both Oxisols was

predominant within this suction interval. The main curves were repeated at least twice and periodically retraced. Assuming negligible changes in the pore geometry or fluidity of the permeating liquid, the main curves should be retracable after the initial main desorption scan was completed. The main curves defined the hysteretic region between which an infinite number of scanning curves could be drawn.

To determine absorption scanning curves, the soil was initially drained along the main desorption curve and then rewetted from suction values less than 200 cm to zero suction. By following the main desorption curve and rewetting the soil at different suction values, a family of absorption scanning curves could be generated.

A similar procedure was used to obtain the desorption scanning curves. The soil was drained to the maximum suction then rewetted at different points along the main absorption curve. Starting at a value less than zero suction, a desorption scanning curve was determined by gradually increasing suction to the maximum of 200 cm. All of the absorption scanning curves have a common end point at zero suction, while the common end point for the desorption scanning curves was the maximum suction of the main desorption curve.

An IBM 360 computer was used to store and convert information corresponding to column position, suction, absorption or desorption history and attenuated intensities in terms of water content and suction data. An "eyeball" best fit curve was plotted through suction or pressure head and soil-water content values for each scan. Points on the non-statistical best fit curves were used in the calculations to approximate the curvature of the hysteresis relationship.

Initial approximations of  $\phi_0$  and  $\beta$  can be obtained by explicitly solving equation (1) for both  $\phi_0$  and  $\beta$  such that

$$\phi_0 = \phi / \left\{ \cosh^{-1} \left[ \frac{(\cosh \epsilon)(\theta_0 - \theta_r)(\theta_0 + \theta) - \epsilon}{(\theta_0 + \theta_r)(\theta_0 - \theta)} \right] \right\} \quad (4)$$

and

$$\beta = \frac{\ln \left\{ \cosh^{-1} \left[ \frac{(\cosh \epsilon)(\theta_0 - \theta_r)(\theta_0 + \theta) - \epsilon}{(\theta_0 + \theta_r)(\theta_0 - \theta)} \right] \right\}}{\ln(\phi/\phi_0)} \quad (5)$$

respectively.

Parameter  $\epsilon$  cannot be solved directly but can be approximated by selecting values which will make the difference of

$$\cosh \epsilon - \frac{(\theta_0 - \theta)(\theta_0 + \theta_r) \cosh [(\phi/\phi_0)^\beta + \epsilon]}{(\theta_0 + \theta)(\theta_0 - \theta_r)} \quad (6)$$

approaches zero.

The three unknown parameters determine the general curvature of the calculated hysteretic function. By selecting two or more points which were representative of the general shape of a single experimentally determined hysteresis curve, values of  $\phi_0$ ,  $\beta$  and  $\epsilon$  could also be estimated. However, since the three parameters were inter-dependent, a large number of combinations of these three parameters were required in order to numerically solve equation (1) for a single scanning curve. Computation time was decreased by roughly estimating the unknown parameters first using the method described above. The calculated curve could then be compared to the experimental data by the difference of least squares method. This method minimized the sum of squares of the differences between the calculated  $\theta$  as compared to the experimental  $\theta$ . An iterative procedure which decreased the interval size between each of the estimated parameter values was then used to find a combination which yielded the

smallest least square value. Each scanning curve could then be characterized by a set of values for  $\theta_0$ ,  $\theta_r$ ,  $\phi_0$ ,  $\beta$  and  $\epsilon$ . Other scanning curves could be predicted from equation (1) if a functional relationship was shown to exist between  $\theta_r$  and either  $\phi_0$  or  $\beta$  for absorption and between  $\theta_0$  and either  $\phi_0$  or  $\beta$  for desorption.

## RESULTS AND DISCUSSION

### Experimental Hysteresis Data

Hysteresis data for the Molokai and Wahiawa soils are presented in Figures 2, 3, 4 and 5. Figures 2 and 4 are absorption scanning curves, and Figures 3 and 5 are desorption scanning curves for both soils, respectively. The data to be reported in this and the following sections are for a single given position or site on the 20 cm long soil column for both soils. For the Molokai soil, the position examined is 9 cm from the top while that for the Wahiawa soil is 10 cm from the top. The data at both of these positions are representative of all positions examined. Data collected at all position would be too voluminous to present here. The number of scanning curves was limited to three absorption and desorption scans because of the time (6 to 10 days) required to complete a single scan.

The Molokai soil was packed to a bulk density of 1.24 g/cc as compared to 0.96 g/cc for the Wahiawa soil. This was due to an initial gravimetric water content of 22% for the Wahiawa soil as compared to the 4% for the Molokai soil. Both were air-dried for 14 days.

The difference in shape between both the desorption and absorption hysteresis curves of the Molokai and Wahiawa soils could be attributed to differences in bulk density due to packing. Furthermore, data presented in Table 1 shows that the Molokai soil has a smaller log mean diameter than the Wahiawa. Hence, it may be surmised that the retention of water by the Molokai soil for suction up to 60 cm is a direct consequence of its higher air entry value which is related to intra-aggregate packing geometry of the soil-water system of both Oxisols.

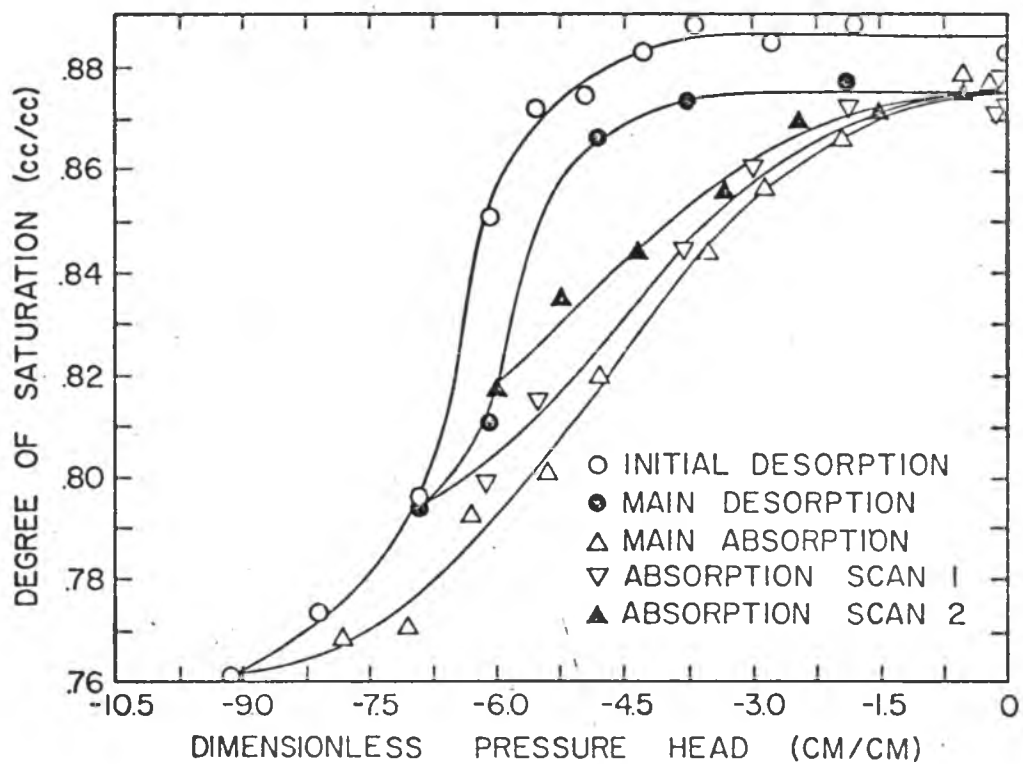


Figure 2. Water Absorption Curves of the Molokai Soil (Typic Torrox) at L=9 cm. The solid line is the "eyeball" best fit curve.

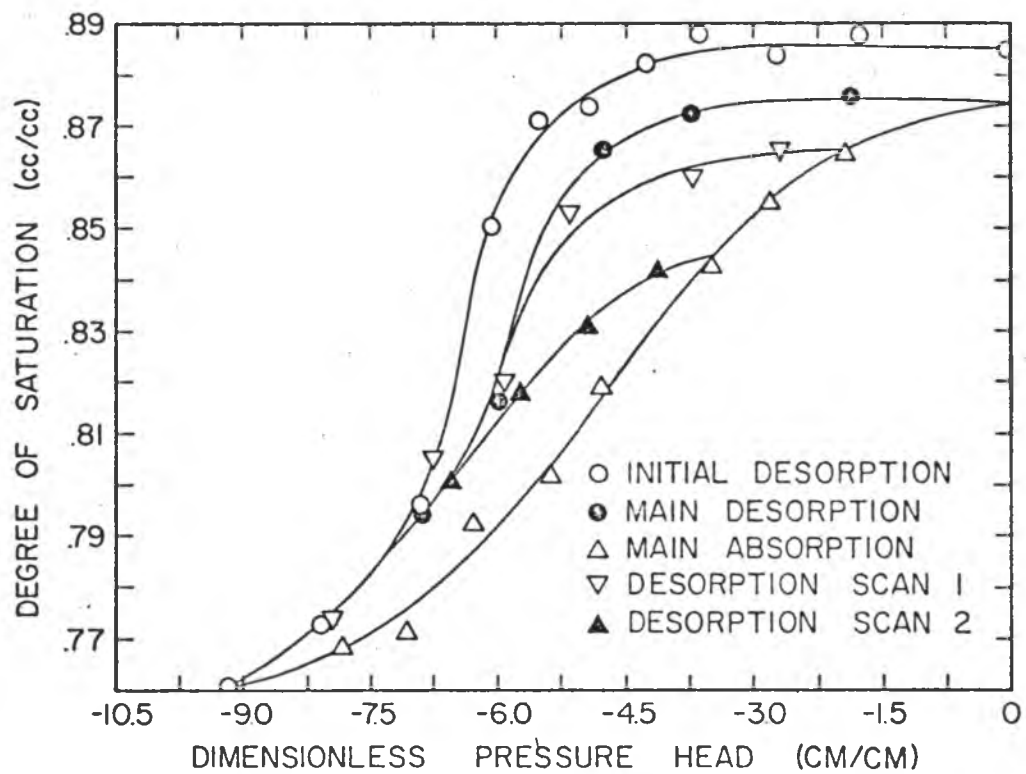


Figure 3. Water Desorption Curves of the Molokai Soil at L=9 cm.

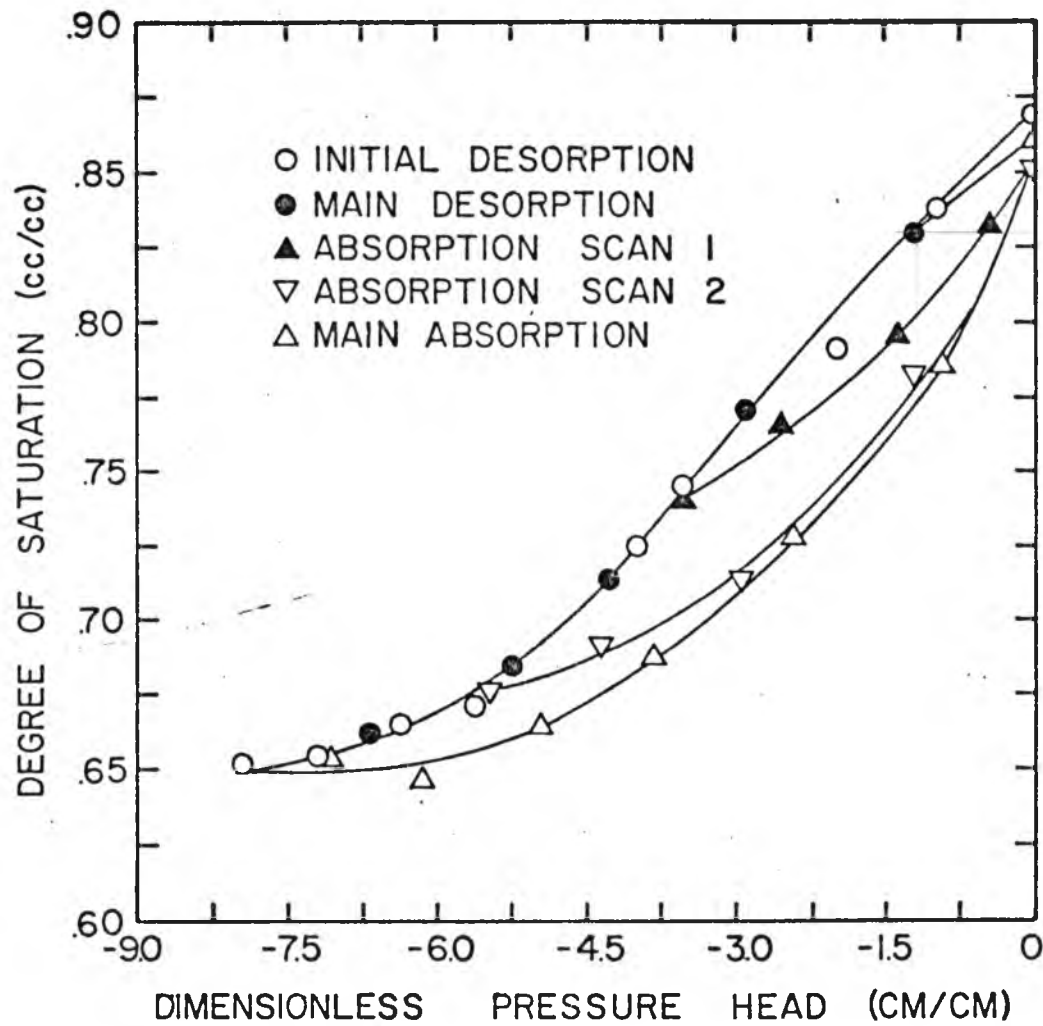


Figure 4. Water Absorption Curves of the Wahiawa Soil (Tropeptic Eutruxox) at L=10 cm. The solid line is the "eyeball" best fit curve.

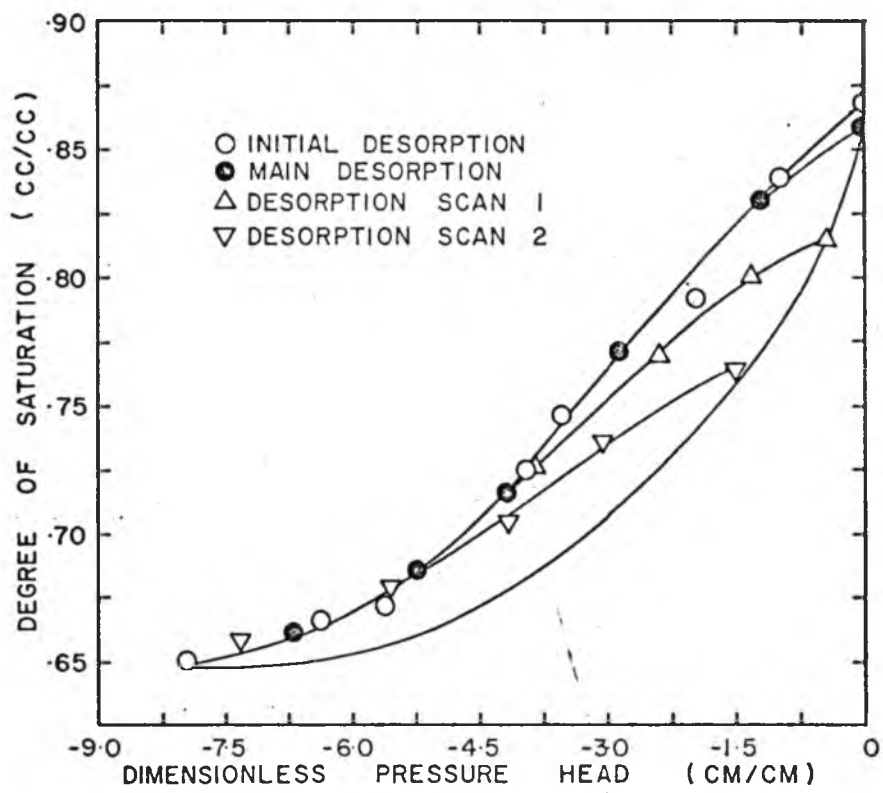


Figure 5. Water Desorption Curves of the Wahiawa Soil at L=10 cm.

Maximum differences in soil-water content due to hysteresis effects for Molokai and Wahiawa soils were 5% and 7%, respectively. For the wetting curves, data points tended to be variable as saturation was approached. An "eyeball" best fit line was drawn through these points.

After the initial desorption from 0 to 200 cm of suction, the main absorption and desorption curves were determined. Both were found to be reproducible. This is a good indication of the stability of soil aggregates of both Oxisols and their ability to maintain their packing configuration with respect to inter-aggregate voids as both soils undergo cycles of wetting and drying. Before each secondary scan was determined, the reproducibility of both main curves was checked.

#### Experimental versus Calculated

Comparisons between experimental curves and those calculated with equation (1) are graphically shown in Figures 6 and 7 for the Molokai soil, in Figure 8 and 9 for the Wahiawa soil and in Figures 10 and 11 for a sandy loam soil (Topp, 1969). The solid lines represent the calculated curves.

For each of the figures, the degree of saturation (volumetric water content in the case of Topp's data) could not be calculated for  $\phi$  greater than -1.5. The quantity  $\cosh[(\phi/\phi_0)^\beta]$  in equation (1) tends towards infinity as the value of  $\phi$  approaches zero and hence, results in "overflow" in the IBM 360 computer output. Furthermore, at  $\phi=0$ ,  $\theta$  cannot be determined since equation (1) is undefined at that point. Between 0 and 30 cm of suction ( $\phi = -1.5$  to 0), water content differences due to hysteresis were significant for both Molokai and Wahiawa soils. This was especially evident in the Wahiawa soil and may be attributed to its

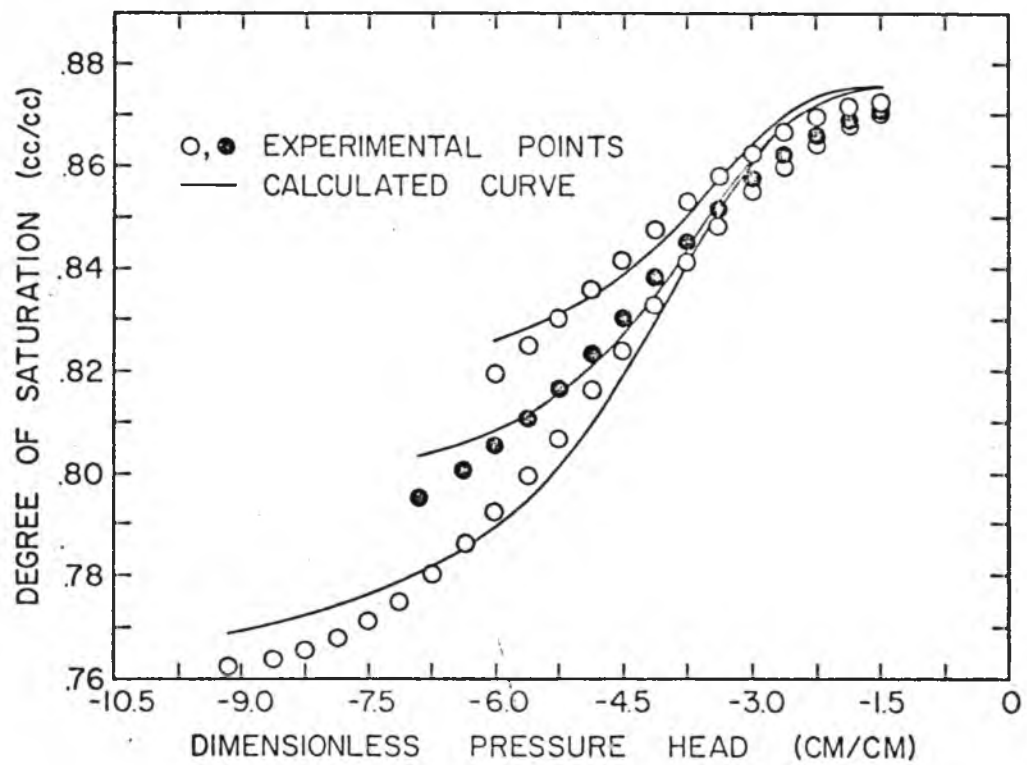


Figure 6. Calculated and Experimental Absorption Curves of the Molokai Soil.

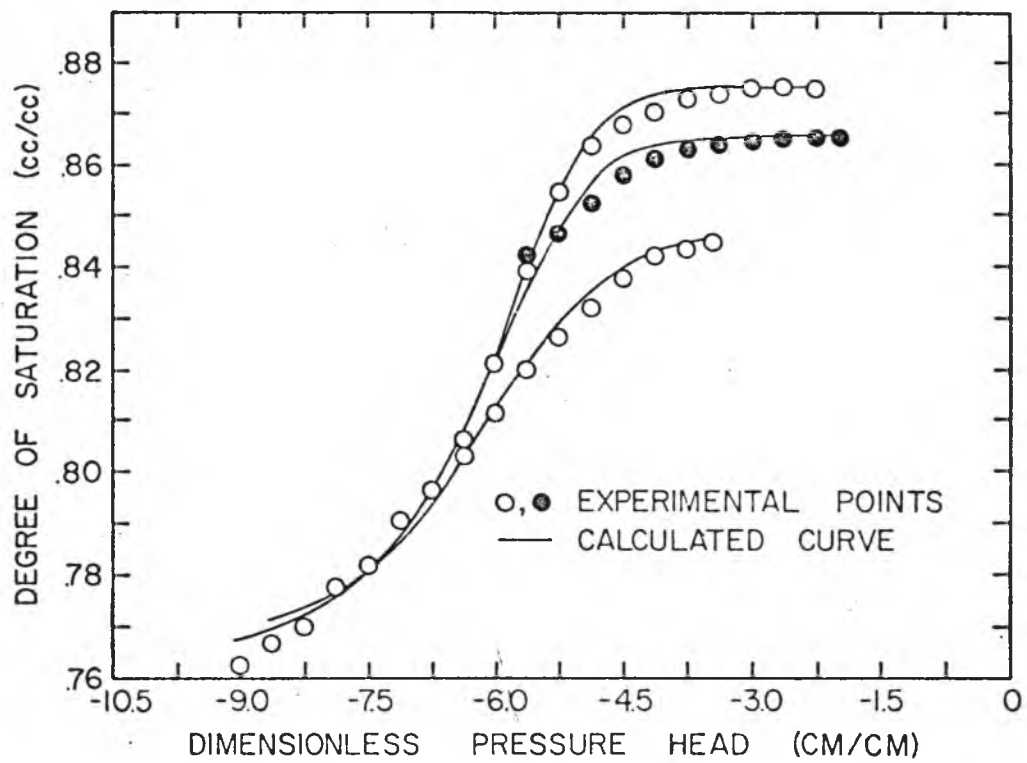


Figure 7. Calculated and Experimental Desorption Curves of the Molokai Soil.

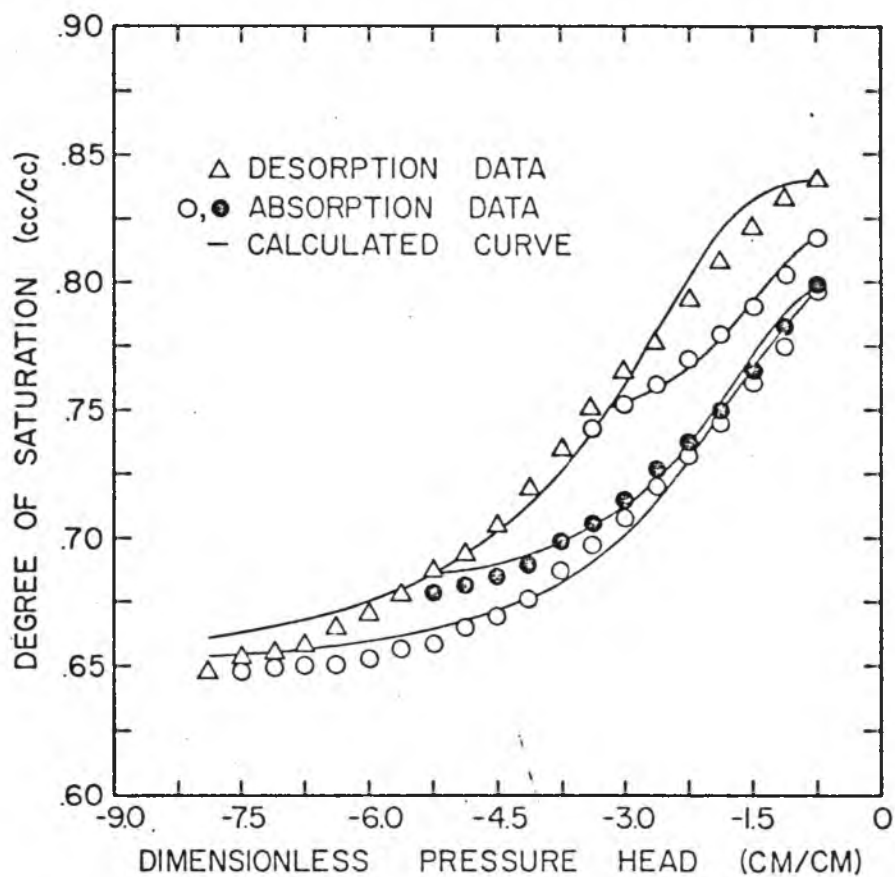


Figure 8. Calculated and Experimental Absorption Curves of the Wahiawa Soil.

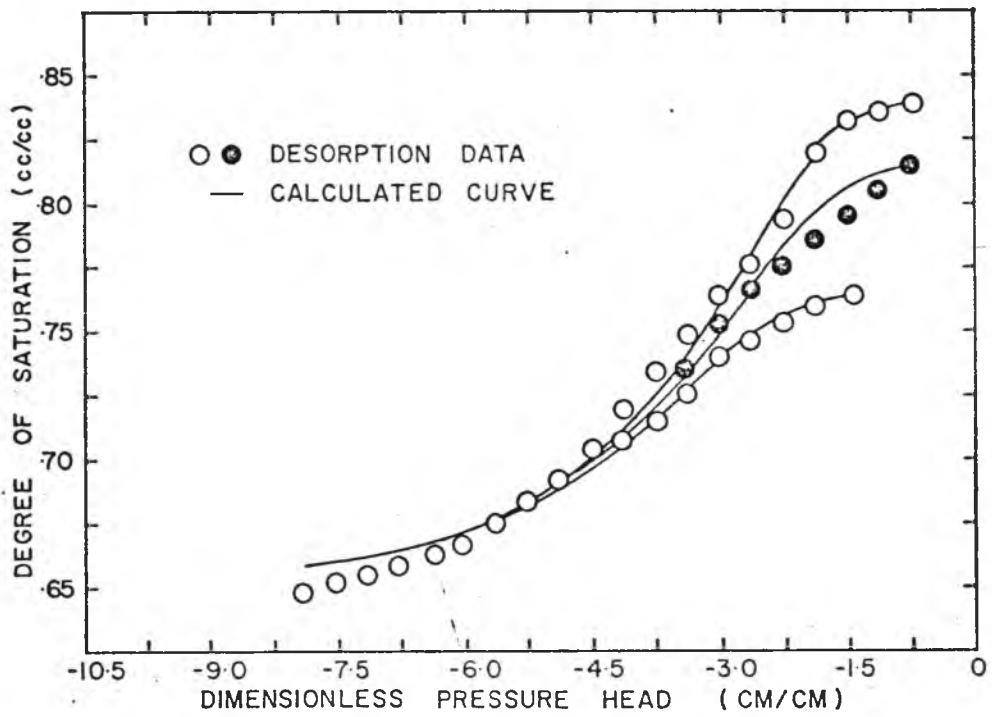


Figure 9. Calculated and Experimental Desorption Curves of the Wahiawa Soil.

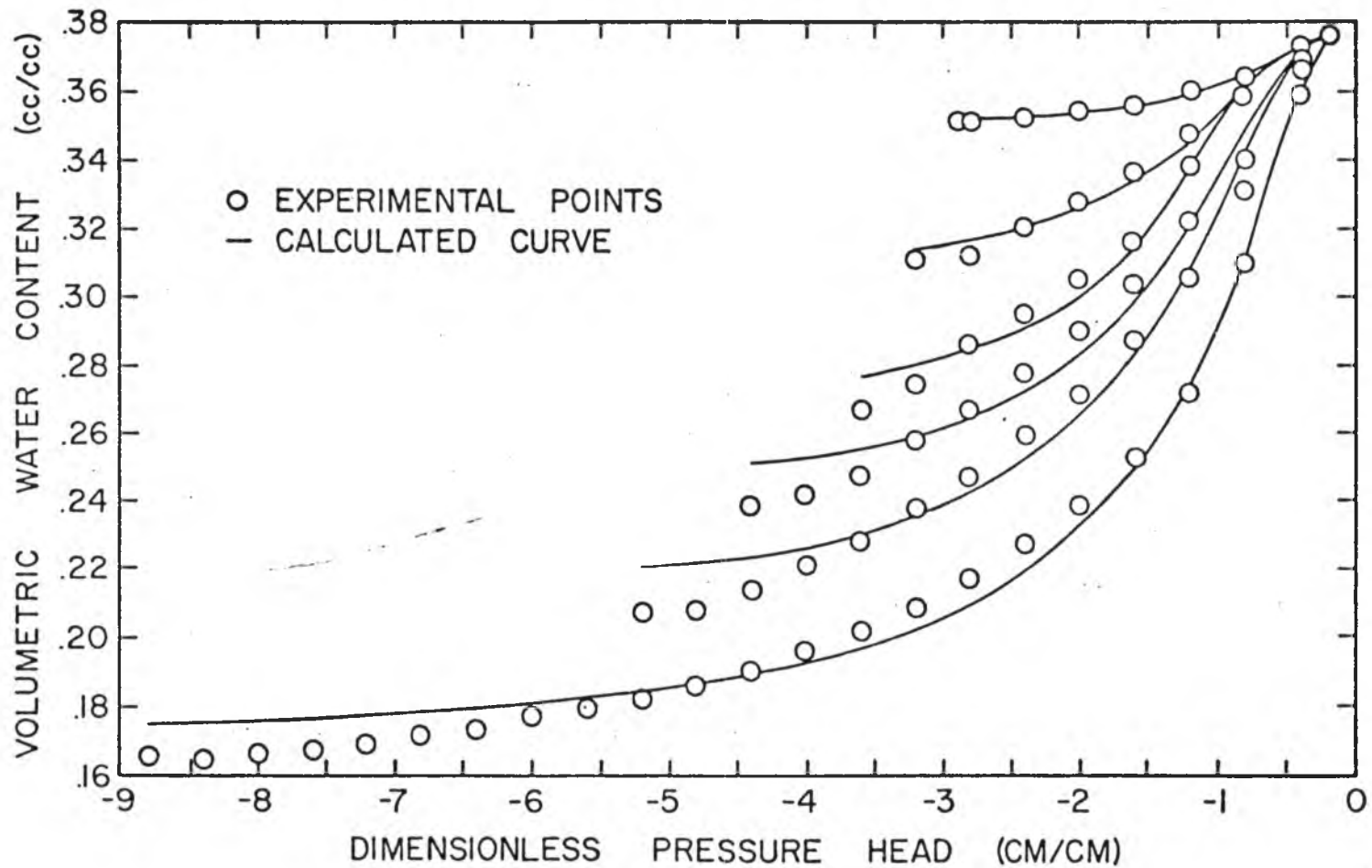


Figure 10. Calculated and Experimental Absorption Curves of the Sandy Loam Soil (from Tcpp, 1969).

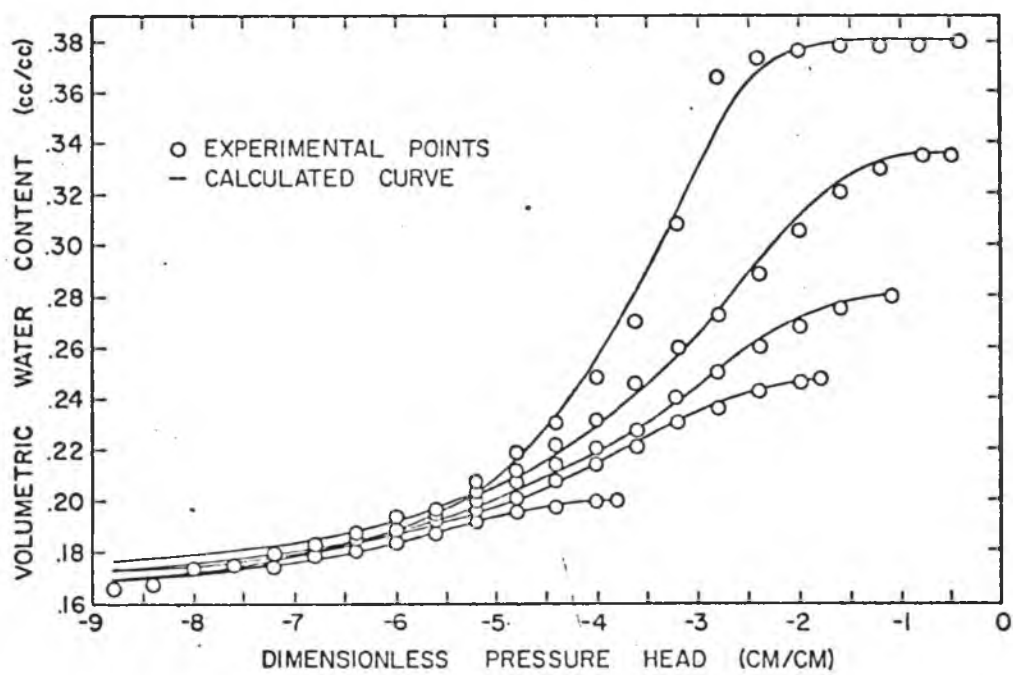


Figure 11. Calculated and Experimental Desorption Curves of the Sandy Loam Soil (Topp's data).

lower air entry value (Tsuji, 1967). In this small pressure interval, the hysteresis data could be approximated by a straight line function where the slope and intercept would be the fitting parameters.

From the general appearance of the computed curves in Figures 6 to 11, a better fit between calculated and experimental was obtained for the desorption curves in comparison to that for the absorption curves. Analogous to experimental curves, calculated desorption curves tended to plateau at constant water contents corresponding to the maximum and minimum pressure heads of each scan. Calculated water content values for the absorption curves, however, continued to increase rather than to plateau at some constant water content as zero suction was approached.

The curve fitting error was usually small for both absorption and desorption. The poorest fit of predicted to experimental occurred at the end points or "tails" of the curves where the maximum water content error was 0.005 cc/cc. When data points on the "eyeball" best fit experimental curve were used instead of actual experimental points, a smoother predicted curve was obtained. All experimental hysteresis curves could be adequately described by equation (1) once the fitting parameters and the linear approximation for  $\phi > -1.5$  were determined. Application of this technique to Topp's data, resulted in an improved fit of experimental to calculated data in comparison to the independent domain theory. Since more scanning curves could be obtained from Topp's (1969) data, functional relationships, if any, between the five curve fitting parameters of equation (1) could be established as discussed in the following section.

### Parameter Relationships

For the absorption process,  $\theta_0$  (approximated by the saturated water content) is a constant for the main and scanning curves and  $\theta_r$ , the residual water content, is dependent on the water content at the point of departure from the main desorption curve. In the case of desorption, on the other hand,  $\theta_r$  is constant and  $\theta_0$  is defined by the water content at the point of departure from the main absorption curve.

Parameters  $\theta_0$  and  $\theta_r$  define the upper and lower boundaries of the degree of saturation or water content, respectively, for a single scanning curve. The calculated scanning curve was forced through the upper boundary at  $\theta_0$  by equation (1). The parameters  $\beta$ ,  $\phi_0$  and  $\epsilon$  determine the shape of that calculated curve and will be discussed in this section. Due to the nature of equation (1), the function yielded better calculated results for experimental data characterized by water content values which levels off to a constant water content at the "tail" of the lower and upper boundaries of a scanning curve. If the data were different from that described, overestimation of water content resulted at these end points. The absorption and desorption calculated curves resulted in similar fitting errors at the lower water contents. Calculated desorption curves, however, gave a better match than the absorption curves which may be attributed to the significant air-entry effects in the Molokai curves. Absorption water content values monotonically increased as zero suction was approached.

Any functional relationship between  $\theta_0$  and either  $\beta$  or  $\phi_0$  for absorption and between  $\theta_r$  and either  $\beta$  or  $\phi_0$  for desorption is of interest. If relationships between these parameters exist, then other scanning curves can be predicted.

## Absorption Curves

A functional relationship between  $\theta_r$  and either  $\beta$  or  $\phi_0$  was obtained from the experimental water content versus pressure head data of the Molokai and Wahiawa soils (Figures 12 and 13). The slopes were positive for  $\theta_r$  versus  $\phi_0$  and negative for  $\theta_r$  versus  $\beta$ . These relationships were similar to those obtained by Gillham (1973). With Topp's (1969) data, however, a non-linear relationship resulted when  $\theta_r$  was plotted against either  $\beta$  or  $\phi_0$  (Figure 14). Deviations from linearity were generally observed when the shape of the experimental scanning curve tended to become horizontal. For scanning curves similar in shape to the absorption curve, as in the case of the two Oxisols, the  $\beta$  or  $\phi_0$  versus  $\theta_r$  relationship was linear. The non-linear relationship between these parameters for Topp's data could probably be described by either an exponential or power function.

By allowing  $\epsilon = 0$ ,  $\theta_0 = \theta_s$  (at zero suction),  $\beta = f(\theta_r)$  and  $\phi_0 = f(\theta_r)$  and by selecting  $\theta_r$  values along the main desorption curve, a family of absorption scanning curves could be generated with the use of equation (1).

## Desorption Curves

For desorption,  $\theta_r$  was constant and a variable  $\theta_0$  was plotted against either  $\beta$  or  $\phi_0$  (Figure 15 and 16). Linear relationships, similar to those in Figure 12 were obtained for the Molokai soil. For the Wahiawa soil, the  $\theta_0$  versus  $\beta$  and  $\theta_0$  versus  $\phi_0$  functions had greater curvature and opposite (negative) slope, respectively, as compared to identical parameter relationships for the Molokai soil.

Gillham (1973) reported non-linear relationships between  $\theta_0$  and either  $\beta$  or  $\phi_0$  for the sandy soil used in his study. Calculations from

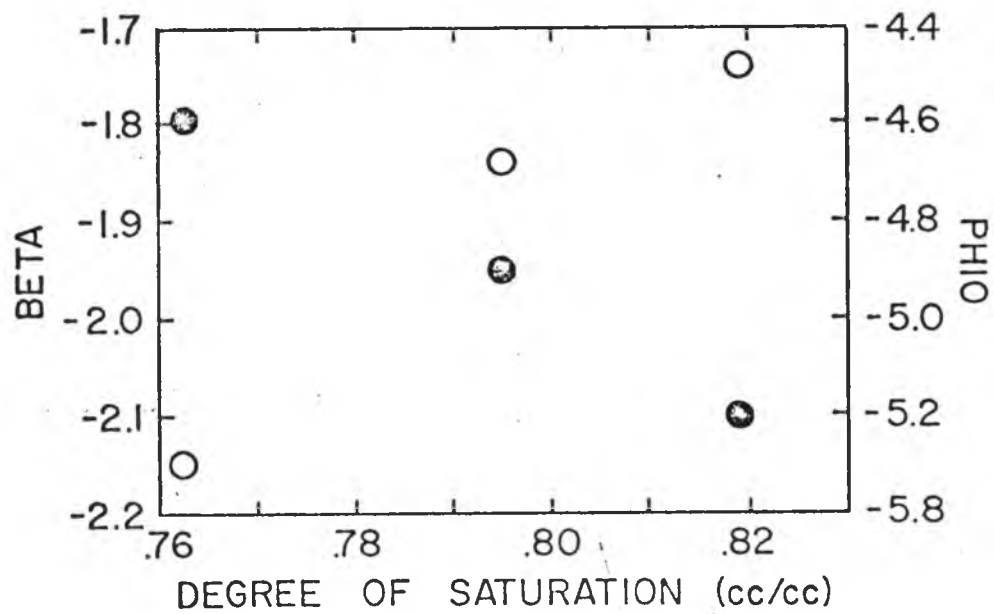


Figure 12. Absorption Fitting Parameters ( $\theta_r$  versus  $\beta$  or  $\phi_0$ ) of the Molokai Soil.  $\beta$  is the solid circle and  $\phi_0$  the open circle.

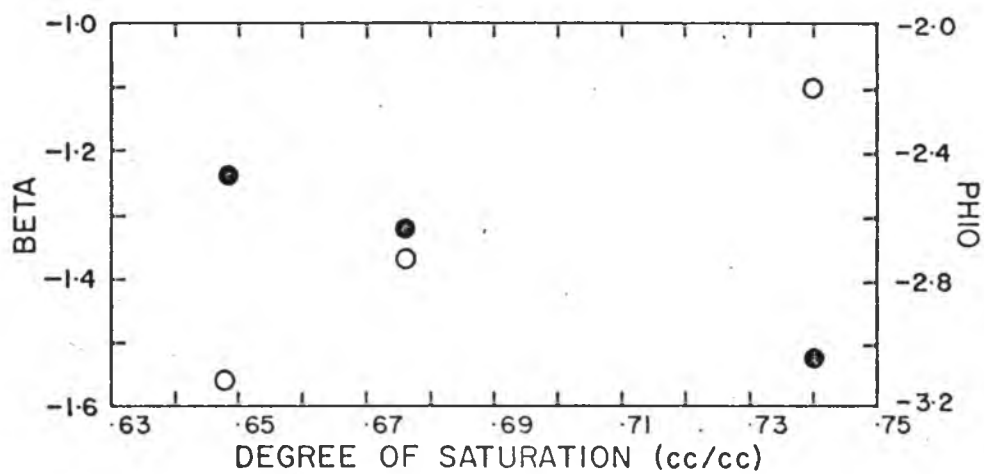


Figure 13. Absorption Fitting Parameters ( $\theta_r$  versus  $\beta$  or  $\phi_0$ ) of the Wahiawa Soil.  $\beta$  is the solid circle and  $\phi_0$  the open circle.

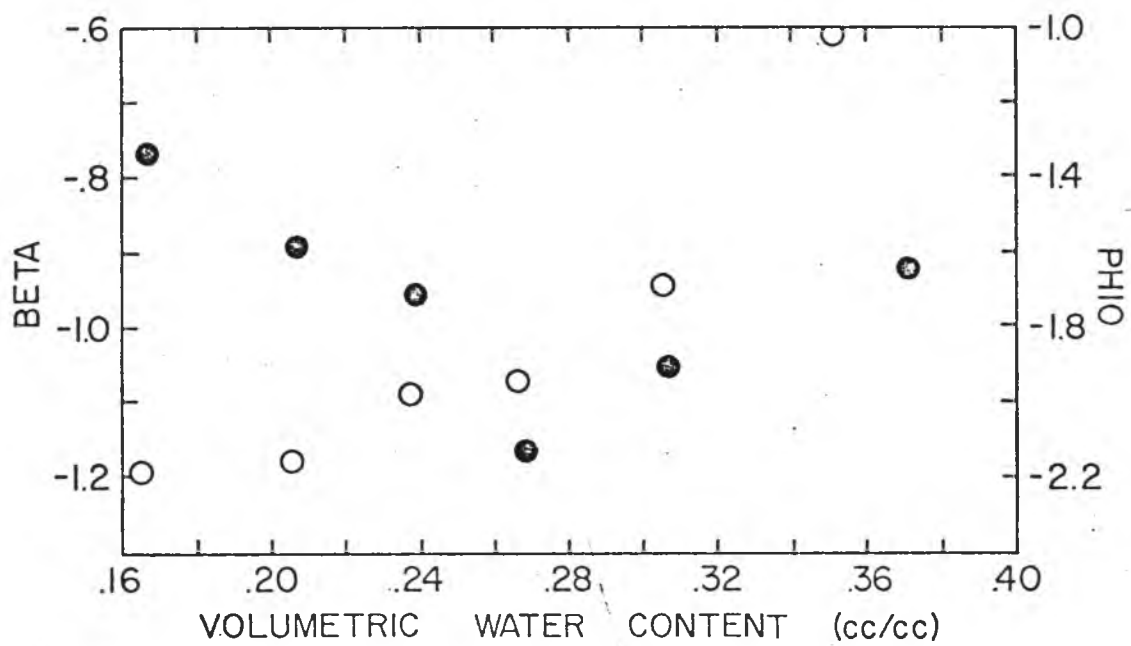


Figure 14. Absorption Fitting Parameters ( $\theta_r$  versus  $\beta$  or  $\phi_0$ ) of Topp's Data.  $\beta$  is the solid circle and  $\phi_0$  the open circle.

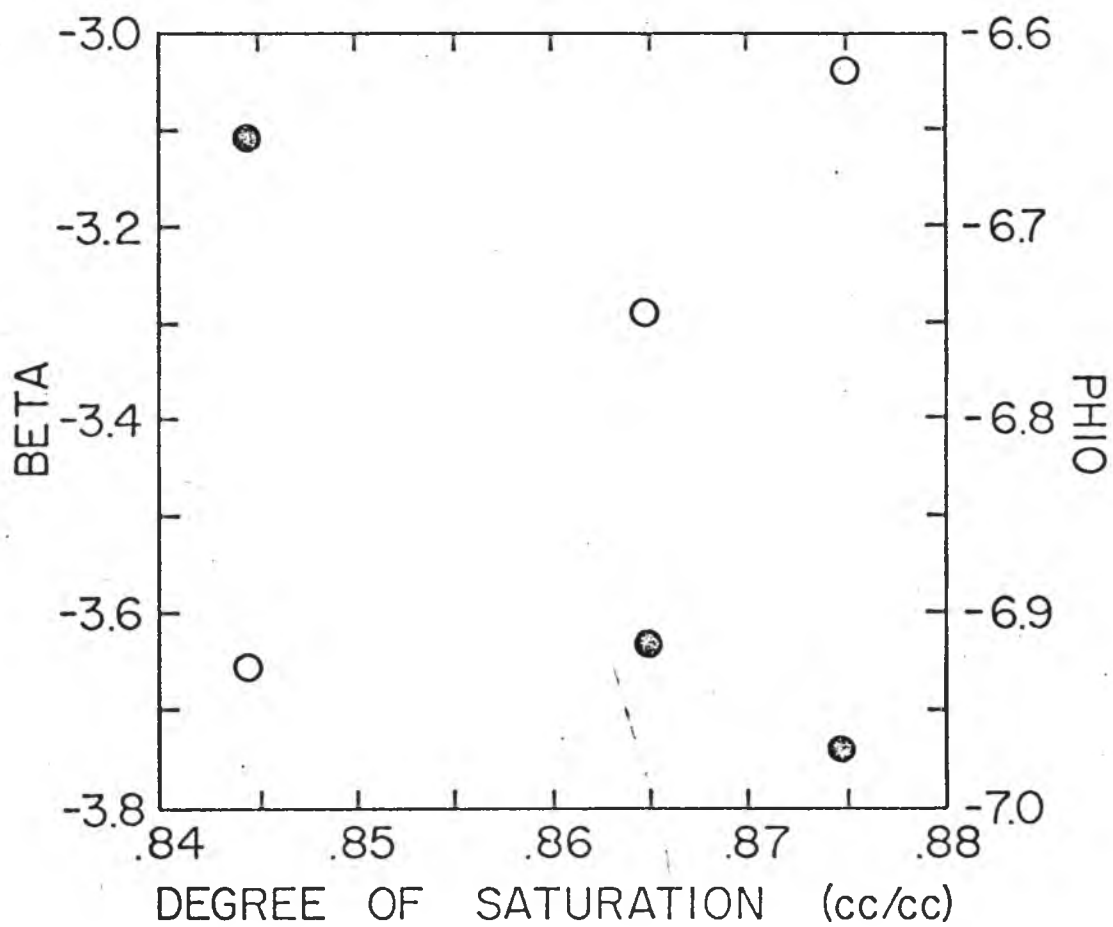


Figure 15. Desorption Fitting Parameters ( $\theta_0$  versus  $\beta$  or  $\phi_0$ ) of the Molokai Soil.  $\beta$  is the solid circle and  $\phi_0$  the open circle.

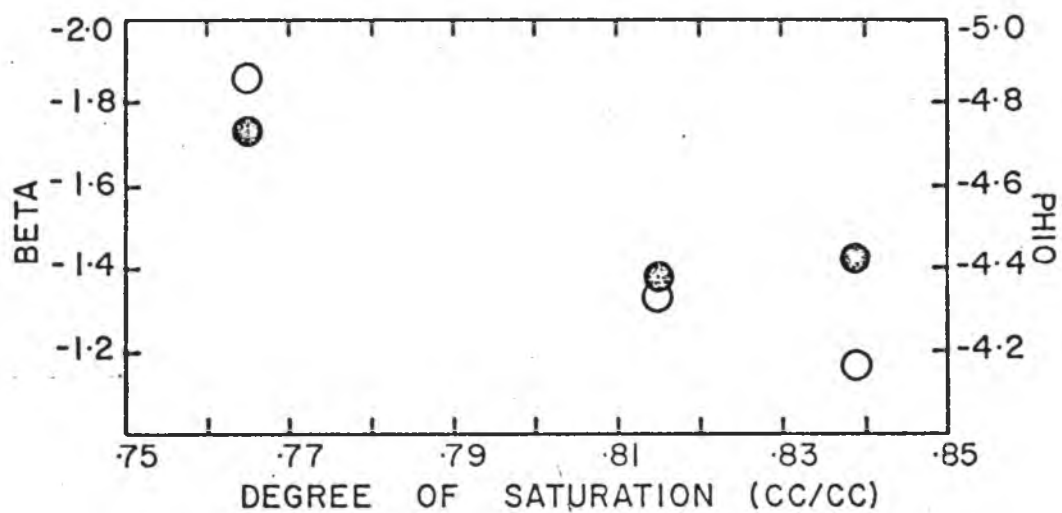


Figure 16. Desorption Fitting Parameters ( $\theta_0$  versus  $\beta$  or  $\phi_0$ ) of the Wahiawa Soil.  $\beta$  is the solid circle and  $\phi_0$  the open circle.

Topp's (1969) data yielded similar results (Figure 17). The plots of  $\theta_0$  and  $\beta$  or  $\phi_0$  were nearly identical in shape to those of Gillham's.

Deviation from linear regression of  $\theta_0$  versus either  $\beta$  or  $\phi_0$  increased as the shape of the scanning curves became more horizontal. By setting the fitting parameters  $\epsilon=0$ ,  $\beta=f(\theta_0)$ ,  $\phi_0=f(\theta_0)$ ,  $\theta_r$  to the residual water content on the main desorption curve and by selecting a  $\theta_0$  (the water content at the point of departure from the main absorption curve), a single desorption scanning curve was generated. All the desorption scans connecting the main curves could then be estimated.

#### Predicted Scanning Curves for the Molokai Soil

Predicted scanning curves for both the absorption and desorption cycles of the Molokai soil are presented in Figures 18 and 19, respectively. Three scanning curves were determined by pointwise solution of equation (1) for selected  $(\phi, \theta)$  values, and by using estimated fitting parameters obtained from Figures 12 and 15. Except for the substitution of  $\theta_0$  for  $\theta_r$  or vice versa in equation (1), computation procedures to determine scanning curves for both absorption and desorption were similar. Hence, discussion of the absorption prediction procedure will suffice.

In the absorption process,  $\epsilon=0$  and  $\theta_0=.8750$  ( $\theta_0=\theta$  at saturation) for all scans between and including the main curve. The functional relationship between  $\theta_r$  and either  $\beta$  or  $\phi_0$  can be expressed as

$$\beta = -5.214 \theta_r + 2.180 \quad (7)$$

and

$$\phi_0 = 14.88 \theta_r + 16.62 \quad (8)$$

from the experimental data in Figures 12 and 15, respectively. The degree of saturation,  $\theta$ , at the point of departure from the main desorption

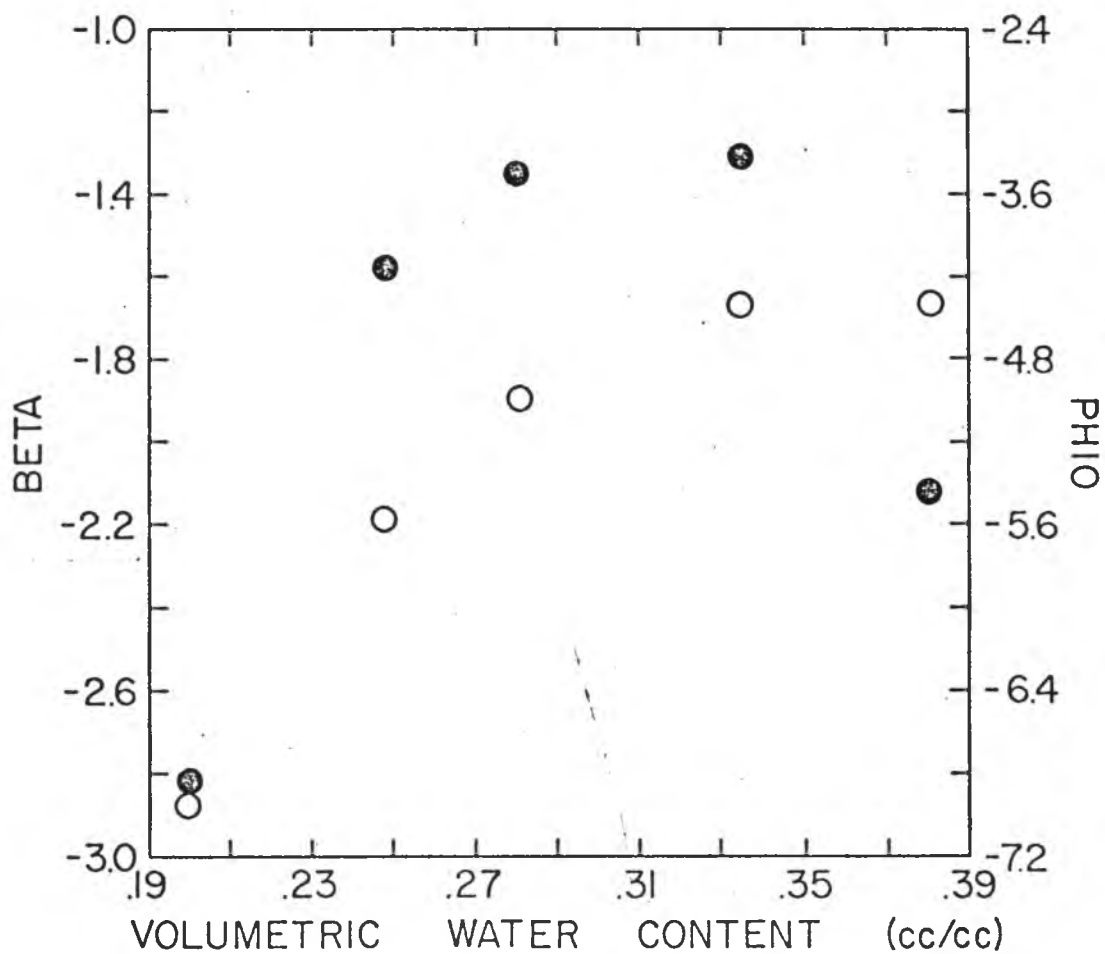


Figure 17. Desorption Fitting Parameters ( $\theta_0$  versus  $\beta$  or  $\phi_0$ ) of Topp's Data.  $\beta$  is the solid circle and  $\phi_0$  the open circle.

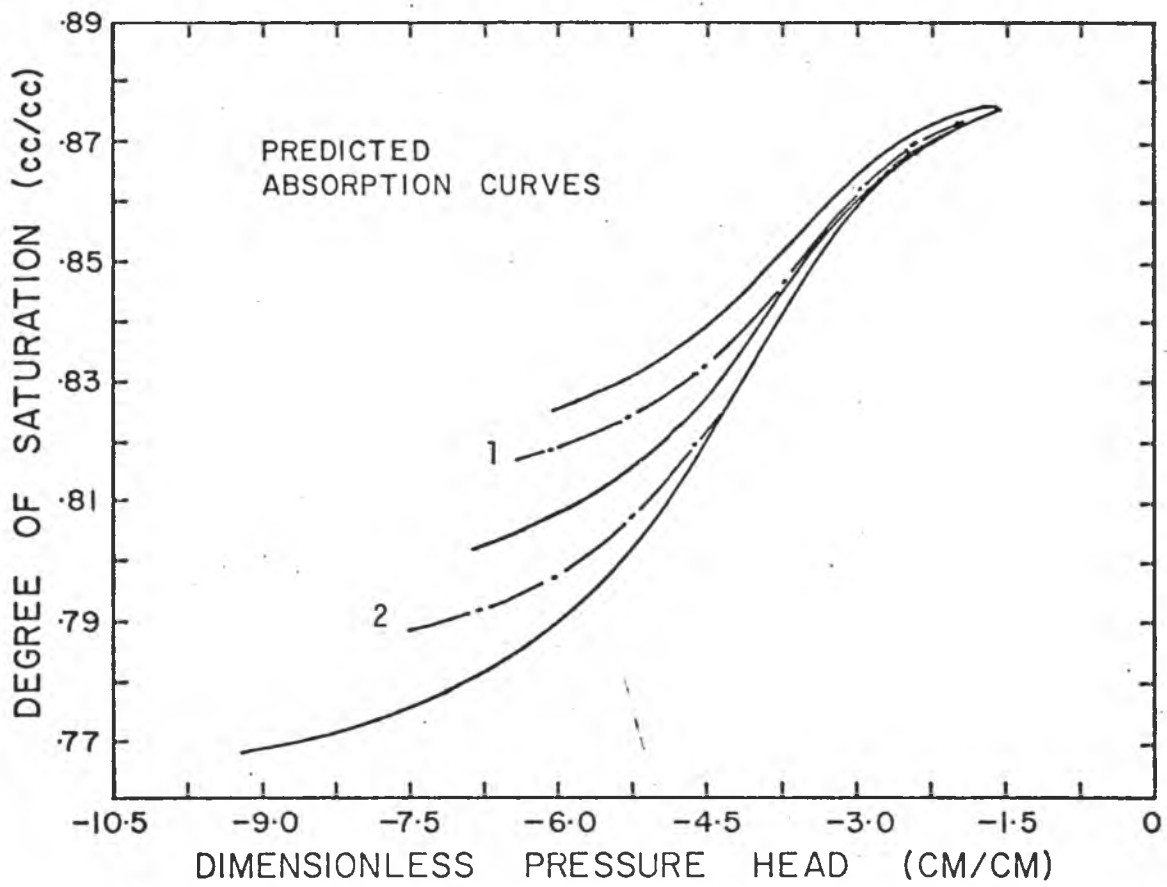


Figure 18. Family of Predicted Absorption Scanning Curves for the Molokai Soil.

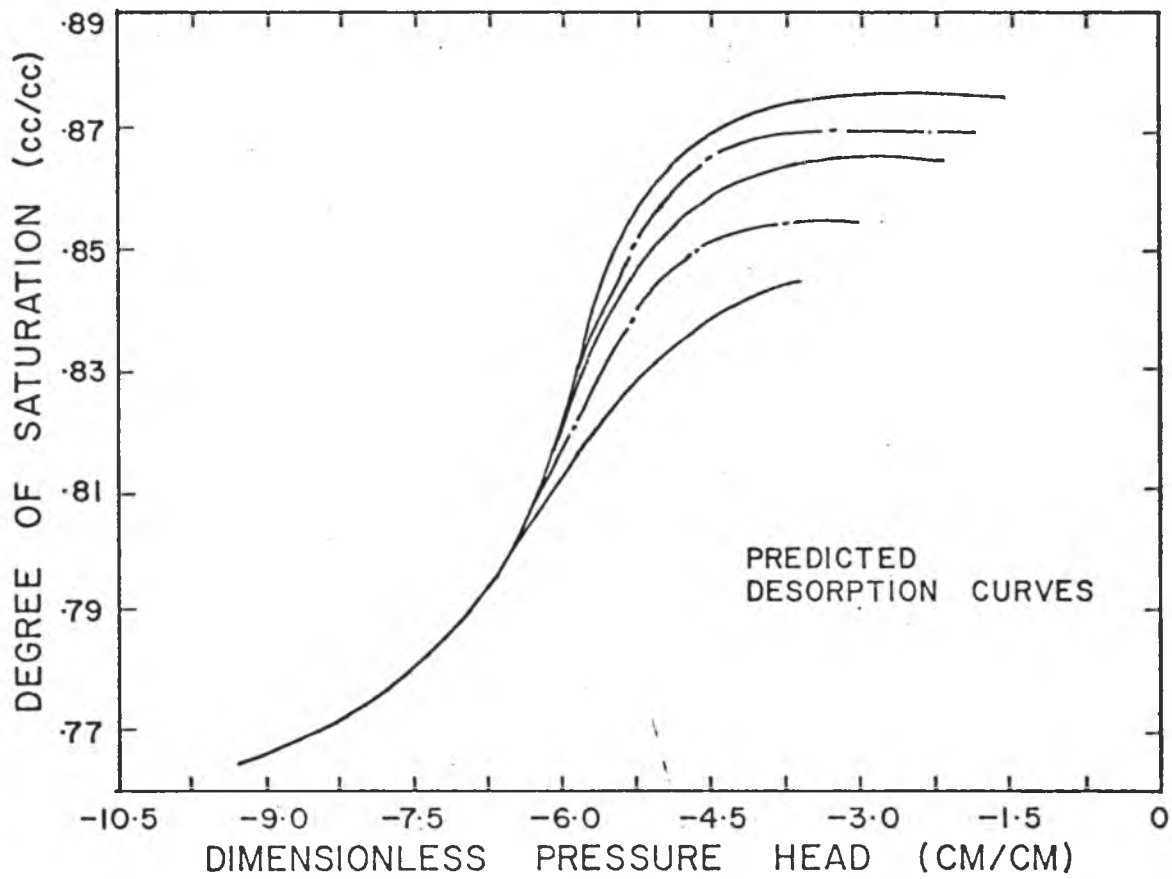


Figure 19. Family of Predicted Desorption Scanning Curves for the Molokai Soil.

curve (i.e. the starting point of the absorption scanning curve) is equal to  $\theta_r$ . Parameters  $\beta$  and  $\phi_0$  can be calculated from equations (7) and (8). When  $\theta_r=.8100$ ,  $\beta=-2.043$  and  $\phi_0=-4.567$ . After the five fitting parameters have been determined, the scanning curve starting from the main desorption curve at ( $\phi=-6.375$ ,  $\theta_r=.8100$ ) can then be determined by using equation (1) to calculate values of  $\theta$ . The symbol  $\phi$  is the independent variable having a range of  $-6.375$  to  $-1.5$ . The result of these calculations are shown in Figure 18 as scan 1. The predicted fitting parameters for the Molokai absorption and desorption scanning curves (dashed lines curves in Figures 18 and 19) are tabulated in Appendix D.

The above procedure may be summarized as follows:

1. Obtain experimental main and at least one secondary scanning curve for either the absorption or the desorption process.
2. Determine curve fitting parameters  $\theta_0$ ,  $\theta_r$ ,  $\phi_0$ ,  $\beta$  and  $\epsilon$  for each scanning curve by iterating equation (1) between a range of "good" estimates for each parameter.
3. Plot and obtain functional relationships of  $\theta_r$  versus  $\beta$  and  $\phi_0$  for absorption, and  $\theta_0$  versus  $\beta$  and  $\phi_0$  for desorption. Parameters  $\theta_0$  and  $\theta_r$  are assumed to be constants for absorption and desorption, respectively. As a good approximation,  $\epsilon$  can be assumed to be zero or close to zero in both processes.
4. Calculate  $\theta$  from equation (1) with the parameters determined in step (2). By choosing the independent variable  $\phi$  in a range between the boundaries of the main curves and calculating  $\theta$  for each  $\phi$ , a scanning curve can be generated.

### Calculated Hydraulic Conductivity

The influence of hysteresis on the relationship between hydraulic conductivity,  $K$ , and suction is much more obvious than that between  $K$  and  $\theta$  (Poulovassilis, 1970; Talsma, 1970; Topp, 1971b). Precise solutions of the unsaturated soil-water flow model require that the function  $K(\theta)$  or  $K(H)$  be known. If the relationships  $\theta(H)$  and  $K(\theta)$  are known,  $K(H)$  can be indirectly determined.

The functional relationship  $K(\theta)$  can be calculated from  $\theta(H)$  by the Kunze et al. (1968) method using main absorption and desorption experimental data of the Molokai and Wahiawa soils (Figures 3 and 5). For the Molokai soil the two main curves were divided into nine equal intervals along the degree of saturation scale for  $\theta$  ranging from .76 to .89. The Wahiawa soil main curves were also divided into nine equal intervals for  $\theta$  ranging from .65 to .87. The Kunze et al. method was programmed similar to that of Harada (1970). This computerized method was employed for calculating the conductivity at corresponding  $\theta$  values for both soils. Figures 20 and 21 are the calculated results for Molokai and Wahiawa soils, respectively. Both plots are comparable to those of Sharma and Uehara (1968). Hysteresis effects on conductivity appear to be small for both soils.

According to Green and Corey (1971), differences between values of conductivity determined by calculation methods may be attributed to the accuracy of the pore size distribution data. They pointed out that the sequence of pore size is more accurately represented by the desorption rather than the absorption curve.

The  $K(H)$  hysteretic relationship for the Molokai soil can be obtained from Figures 20 and 2 for absorption and from Figure 3 for desorption.

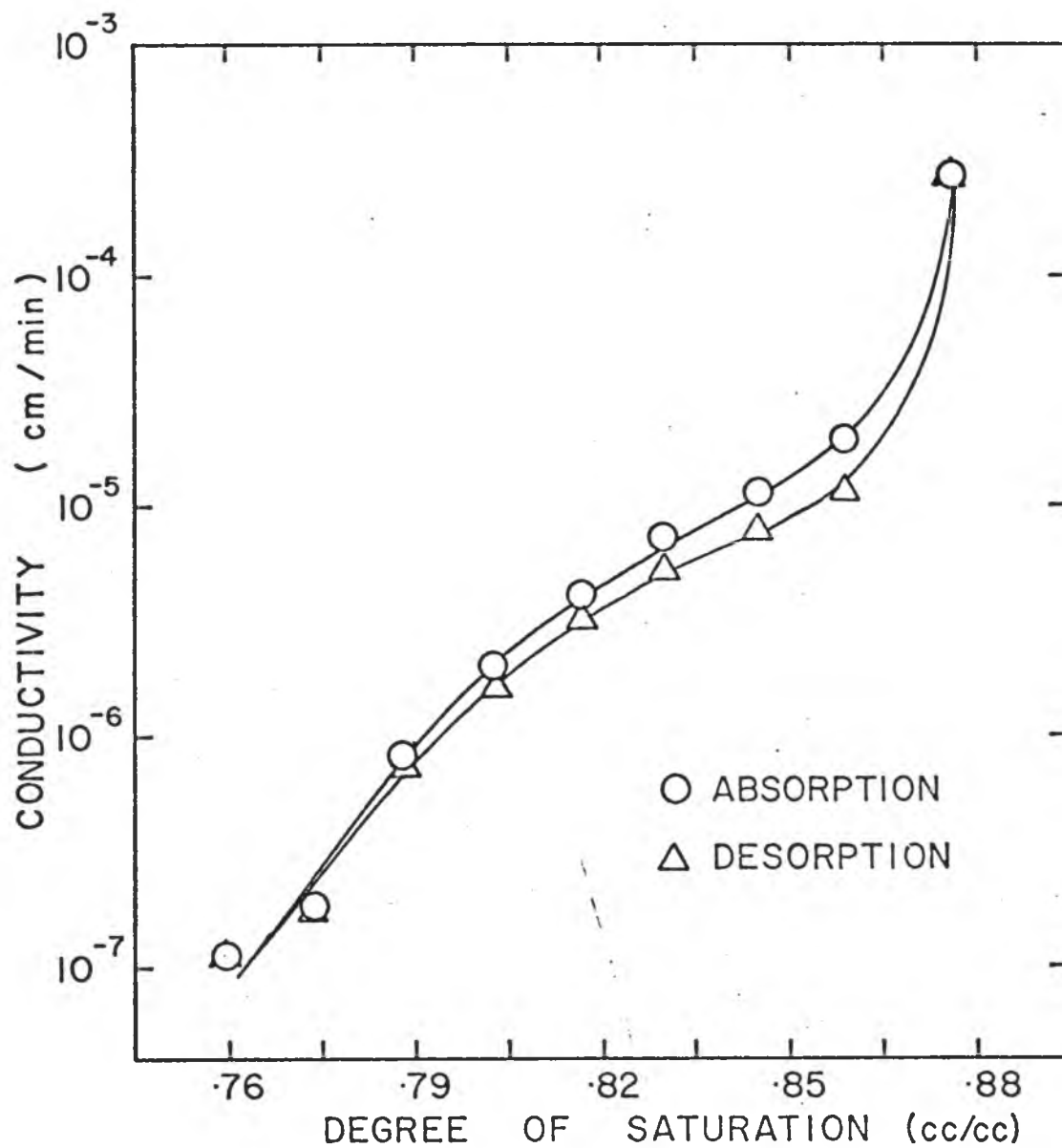


Figure 20. Calculated Conductivity versus Degree of Saturation from Absorption and Desorption Data of the Molokai Soil.

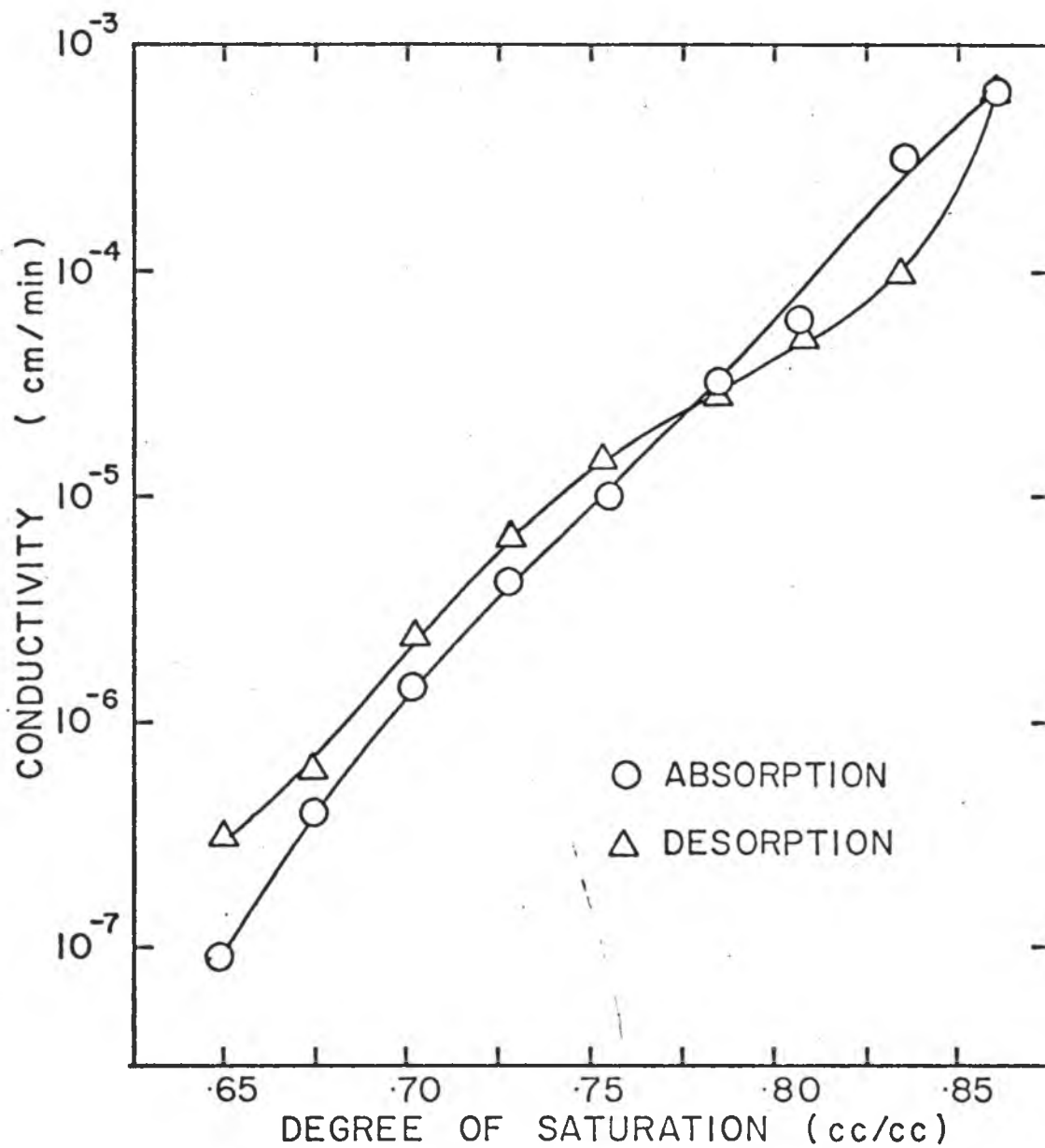


Figure 21. Calculated Conductivity versus Degree of Saturation from Absorption and Desorption Data of the Wahiawa Soil.

Similarly,  $K(H)$  can be determined for the Wahiawa soil from Figures 21 and 4 for absorption and Figure 5 for desorption.

## IMPLICATION OF RESULTS AND SUMMARY

Soil water hysteresis, in most instances, have been neglected in the solution of the flow equation. Published results relating the hysteresis phenomenon to the water transport coefficients have been limited to porous medium of coarse texture. This was understandably due to the greater influence of hysteresis in these coarse textured materials. In several cases, assumed scanning hysteretic curves were used to compute values of unsaturated hydraulic conductivity. This was done primarily because methods to predict hysteretic scanning curves from available water characteristic data were generally unsatisfactory. However, results obtained in this study and that of Klute and Gillham (1973) indicate that the model of King (1965) with modifications (Gillham, 1973) can make reasonable predictions of hysteretic scanning curves. In fact, the modified King equation appears to be well suited for the aggregated oxidic soil materials used here. Prediction of a family of absorption and desorption scanning curves was also possible for a sandy loam soil. The relationship between fitting parameters of the model were not linear in all cases, but the existence of a continuous relationship for the non-linear cases may permit prediction of the necessary fitting parameters to generate a family of scanning curves.

Results obtained in this study may be used in such problems as water redistribution after infiltration. That is, if knowledge of the wetting and drying history of the soil is known, precise predictions of the rate of water movement in terms of soil water diffusivity and unsaturated hydraulic conductivity can be made. With this predictive capability, timing and rate of water application for furrow, sprinkler and even drip irrigation can be optimized for a given distribution of water soil.

Maximum differences in water content due to the effect of hysteresis on the water absorption and desorption characteristics for the Molokai and Wahiawa soils are 5 and 7 percent, respectively. The magnitude of the water content differences for both soils would probably be insignificant when predictions of water movement under field conditions are made.

Prediction of the experimental scanning hysteretic curves by the mathematical model of King (1965) and modified by Gillham (1973) was good for the well-aggregated Oxisols used in this study. This method gave accurate results as compared to the independent model prediction for Topp's sandy loam soil.

The major disadvantage of this method was the complex iteration process in which the inter-dependent fitting parameter (  $\beta$ ,  $\phi_0$  and  $\epsilon$  ) were determined.

## LITERATURE CITED

1. Bomba, S. J., and E. E. Miller. 1967. Secondary scan hysteresis in glass bead media. Agron. Abstr., Annual Meetings. Amer. Soc. of Agron., Washington, D. C., Nov. 5-10. pp. 62.
2. Bomba, S. J. 1968. Hysteresis and time-scale invariance in a glass-bead medium. PhD dissertation. University of Wisconsin.
3. Bresler, E., W. D. Kemper, and R. J. Hanks. 1969. Infiltration, redistribution, and subsequent evaporation of water from soil as affected by wetting rate and hysteresis. Soil Sci. Soc. Amer. Proc. 33:832-840.
4. Cagauan, B., and G. Uehara. 1965. Soil anisotropy and its relation to aggregate stability. Soil Sci. Soc. Amer. Proc. 29: 198-200.
5. Collis-George, N. 1955. Hysteresis in moisture content-suction relationships in soils. Nat. Acad. Sci. Proc. (India) Allahabad. 24A:80-85.
6. Davidson, J. M. 1965. The dependence of soil water uptake and release upon the applied pressure increment. PhD dissertation. University of California (Davis).
7. Enderby, J. A. 1955. The domain model of hysteresis. Part I. Independent domains. Faraday Soc. Trans. 51:835-848.
8. Everett, D. H. 1955. A general approach to hysteresis: Part IV. An alternative formulation of the domain model. Faraday Soc. Trans. 51:1551-1557.
9. Everett, D. H. 1967. Adsorption hysteresis in solid-gas interface in SOLID GAS INTERFACE. vol. 2. Edited by E. Allison Flood, Marcell Decker. New York.
10. Gardner, W. R. 1968. Some steady-state solutions of the unsaturated moisture flow equation with application to evaporation from a water table. Soil Sci. 85:228-232.
11. Gillham, R. W. 1973. Hysteretic water flow in a porous medium: Experimental study and numerical simulation. PhD dissertation. University of Illinois.
12. Green, R. E., and J. C. Corey. 1971. Calculation of hydraulic conductivity: A further evaluation of some predictive methods. Soil Sci. Soc. Amer. Proc. 35:3-8.

13. Haines, W. B. 1930. Studies in the physical properties of soils: V. The hysteresis effect in capillary properties and the modes of moisture distribution associated therewith. *Jour. Agr. Sci.* 20:97-116.
14. Hanks, R. J., A. Klute, and E. Bresler. 1969. A numeric method for estimating infiltration, redistribution, drainage, and evaporation of water from soil. *Water Resour. Res.* 5(5): 1064-1069.
15. Hillel, D. 1971. *Soil and Water, Physical Principles and Processes*. Edited by T. T. Kozlowski, Academic Press. New York.
16. King, L. G. 1965. Description of soil characteristics for partially saturated flow. *Soil Sci. Soc. Amer. Proc.* 29:359-362.
17. Klute, A., and R. W. Gillham. 1973. An experimental study of soil water flow systems involving hysteresis. Completion Report No. 51. Environmental Resources Center, Colorado State University.
18. Kunze, R. J., G. Uehara, and K. Graham. 1968. Factors important in the calculation of hydraulic conductivity. *Soil Sci. Soc. Amer. Proc.* 26:421-426.
19. Miller, E. E., and R. D. Miller. 1956. Physical theory for capillary flow phenomena. *Jour. Appl. Phys.* 27:324-332.
20. Philip, J. R. 1964. Similarity hypothesis for capillary hysteresis in porous materials. *Jour. Geophys. Res.* 69(8):1553-1562.
21. Poulovassilis, A. 1969. The effect of pore water hysteresis on the hydraulic conductivity. *Jour. Soil Sci.* 20:52-56.
22. Poulovassilis, A. 1970. Hysteresis of pore water in granular porous bodies. *Soil Sci.* 109:5-12.
23. Richard, S. J. 1938. Soil moisture content calculations from capillary tension records. *Soil Sci. Soc. Amer. Proc.* 3:57-64.
24. Sharma, M. L. 1966. Influence of soil structure on water retention, water movement and thermodynamic properties of adsorbed water. PhD dissertation. University of Hawaii.
25. Sharma, M. L., and G. Uehara. 1968. Influence of soil structure on water relations in low humic latosols: I. Water retention. *Soil Sci. Soc. Amer. Proc.* 32:765-770.
26. Sharma, M. L., and G. Uehara. 1968. Influence of soil structure on water relations in low humic latosols: II. Water movement. *Soil Sci. Soc. Amer. Proc.* 32:770-774.

27. Smiles, D. E., G. Vachaud, and M. Vauclin. 1971. A test of the uniqueness of the soil moisture characteristic during transient, nonhysteretic flow of water in a rigid soil. *Soil Sci. Soc. Amer. Proc.* 35(4):534-539.
28. Smith, W. O., P. D. Foot, and P. F. Busong. 1931. Capillary rise in sands of uniform spherical grains. *Jour. Appl. Phys.* 1: 18-26.
29. Southard, A. 1974. Personal communications with Al Southard, Visiting Professor of Agronomy and Soils Department, University of Hawaii.
30. Staple, W. J. 1969. Comparison of computed and measured moisture redistribution following infiltration. *Soil Sci. Soc. Amer. Proc.* 33:840-847.
31. Staple, W. J. 1970. Predicting moisture distribution in rewetted soils. *Soil Sci. Soc. Amer. Proc.* 34:387-392.
32. Talsma, T. 1970. Hysteresis in two sands and the independent domain model. *Water Resour. Res.* 6(3):964-970.
33. Topp, G. C. 1964. Hysteretic moisture characteristics and hydraulic conductivities for glass bead media. PhD dissertation. University of Wisconsin. Univ. Microfilm, Ann Arbor, Mich. (diss. Abstr. 25:3629).
34. Topp, G. C., and E. E. Miller. 1966. Hysteretic moisture characteristics and hydraulic conductivity for glass-bead media. *Soil Sci. Soc. Amer. Proc.* 30:156-162.
35. Topp, G. C. 1969. Soil-water hysteresis measured in a sandy loam and compared with the hysteretic Domain Model. *Soil Sci. Soc. Amer. Proc.* 33:645-651.
36. Topp, G. C. 1971a. Soil-water hysteresis: The domain model extended to pore interaction conditions. *Soil Sci. Soc. Amer. Proc.* 35:219-225.
37. Topp, G. C. 1971b. Soil water hysteresis in silt loam and clay loam soils. *Water Resour. Res.* 7(4):914-920.
38. Tsuji, G. Y. 1967. Measurement and evaluation of soil water transmission coefficients in some Hawaiian Latosols. MS thesis. University of Hawaii.
39. Tsuji, G. Y., R. T. Watanabe, and W. S. Sakai. 1974. Influence of soil micro-structure on water characteristics of selected Hawaiian soils. Submitted to *Soil Sci. Soc. Amer. Proc.*

40. Uehara, G., K. W. Flach, and G. D. Sherman. 1962. Genesis and micro-morphology of certain soil structural types in Hawaiian Latosol and their significance in agricultural practices. Int. Soc. Soil Sci., Trans. Comm. V. A7:3-8.
41. Youngs, E. G. 1960. The hysteresis effect versus soil moisture studies. Int. Cong. Soil Sci. Trans. 7th. 1:107-113.

APPENDIX A

IN SITU WATER CONTENT AND DENSITY MEASUREMENTS  
THROUGH GAMMA-RAY ATTENUATION TECHNIQUES.

## INTRODUCTION

Direct water content measurements in static soil-water characteristic determinations and in transient water flow experiments have primarily been restricted to gravimetric methods. Indirect measurement of water content can be gained by the use of tensiometers, electrical resistance blocks, thermocouple psychrometers, thermistors, etc. Gravimetric procedures generally result in the disturbance of the soil-water system during sectioning, while indirect methods must allow for lag time if precise water content measurements are made. With the advent of gamma-ray attenuation techniques, rapid nondestructive determination of soil bulk density and soil-water content is now possible.

Vomicil (1954), Bernhard and Chasek (1955) and van Bavel et al. (1957) were among the first researchers to use the gamma-ray attenuation technique to measure soil bulk density. Later, Ferguson and Gardner (1962), Gurr (1962) and Davidson et al. (1963) applied this technique to determine water contents in thin layers of soil.

The first gamma-ray attenuation unit in the State of Hawaii for soils work was designed and fabricated by the soil physics group of the Department of Agronomy and Soil Science, University of Hawaii. A theoretical discussion and initial results related to the testing of the gamma-ray unit are presented in this section. Methods and techniques employed here are applicable to similar laboratory or field instrumentation which are now commercially available. Potentially, such instrumentation can be used for in situ water content and density measurements at different soil depths. These determinations will be much more precise than those

obtained by the neutron probe because of the better resolution of the collimated gamma-ray beam.

## THEORY

Fundamental principles of gamma-ray densitometry for monoenergetic primary radiation are based on the attenuation equation which may be expressed as

$$I = I_0 \exp(-\mu \rho x) \quad (1a)$$

where  $I$  is the attenuated intensity of the gamma-ray beam,  $I_0$  is the intensity at the source and  $\mu$ ,  $\rho$  and  $x$  are the mass attenuation coefficient ( $\text{cm}^2/\text{g}$ ), density ( $\text{g}/\text{cm}^3$ ) and thickness ( $\text{cm}$ ) of the attenuating material, respectively.

Equation (1a) can be rewritten as

$$N = N_0 \exp(-\mu \rho x)$$

or 
$$\ln(N_0/N) = \mu \rho x \quad (2a)$$

where  $N$  and  $N_0$  refer to instrument photon counting rates instead of actual intensity. This is valid only if the detector recordings correlate directly with the radiation intensity. Verifying the validity of equation (2a) is synonymous to experimentally demonstrating that a proportional relationship exists between  $\ln(N_0/N)$  and  $\rho$  or  $x$ .

For single component systems such as pure water or dry soil, equation (2a) can be applied directly by substituting in the necessary constants. For a multicomponent system such as the one existing in moist soils, the following general relationship is applicable

$$N = N_0 \exp(-\mu_1 \rho_1 x_1 - \mu_2 \rho_2 x_2 - \dots - \mu_n \rho_n x_n) \quad (3a)$$

where  $\mu_1, \dots, \mu_n$ ,  $\rho_1, \dots, \rho_n$  and  $x_1, \dots, x_n$  are the mass attenuation coefficients, densities and the sample thicknesses of each of the individual components, respectively.

For moist soil packed in a plexiglas cylinder, the attenuation equations of interest may be expressed as

$$N_c = N_o \exp(-\mu_c \rho_c x_c) \quad (4a)$$

and

$$N_m = N_o \exp(-\mu_c \rho_c x_c - \mu_s \rho_s x_s - \mu_w \rho_w x_w \theta) \quad (5a)$$

where  $N_c$  is the intensity through the empty plexiglas container,  $N_m$  is the intensity through both moist soil and container,  $\theta$  the volumetric water content, and subscripts c, s and w refer to the plexiglas container, soil and water, respectively. Combining equations (4a) and (5a) yields

$$N_m = N_c \exp(-\mu_s \rho_s x_s - \mu_w \rho_w x_w \theta) \quad (6a)$$

For an oven-dried soil, where  $\theta=0$ , equation (6a) will reduce to

$$N_d = N_c \exp(-\mu_s \rho_s x_s) \quad (7a)$$

where  $N_d$  equals the intensity of the beam transmitted through dry soil. Given either the mean soil bulk density  $\bar{\rho}_s$  or the mean mass attenuation coefficient of soil  $\bar{\mu}_s$ , the other can be calculated by rearranging equation (7a) such that

$$\bar{\mu}_s = \ln(N_c/N_d) / \bar{\rho}_s x_s \quad (8a)$$

and

$$\bar{\rho}_s = \ln(N_c/N_d) / \bar{\mu}_s x_s \quad (9a)$$

The mean bulk density is determined by measuring the mass of soil packed in the plexiglas cylinder of known volume. The mean mass attenuation coefficient can be measured experimentally by varying the mean bulk density in equation (8a).

For water alone, equation (6a) will reduce to

$$N_w = N_c \exp(-\mu_w \rho_w x_w) \quad (10a)$$

which on rearrangement yields

$$\mu_W = \ln(N_C/N_W)/\rho_W x_W \quad (11a)$$

where  $\rho_W$  is the density of water and  $x_W$  the inside dimension of the container. With constants  $\mu_W$ ,  $\rho_W$  and  $x_W$  known, the soil-water content can be calculated at given positions in the soil column. By combining equations (6a) and (7a) to yield

$$\theta = \ln(N_d/N_m)/\mu_W \rho_W x_W \quad (12a)$$

The attenuation equation assumes that the densities of the attenuating materials remain constant at each position in the soil column where the analysis is to be made. Non-isothermal conditions and either expansion or contraction of the soil-water system would result in erroneous data.

Equation (1a) is theoretically valid only for monoenergetic primary radiation that is transmitted to the detector without alterations. Gamma-ray photons interact with the sample by being either absorbed or scattered. Absorption is characterized by the disappearance of a photon while scattered photons are deflected from their original direction either with or without a loss of energy. Energy changes due to either the photoelectric effect, Compton scattering or electron pair production may invalidate the assumption of a monoenergetic radioactive source (Kohl et al., 1961; and King, 1967). In the lower energy range (less than 0.5 MeV), the process of importance is the photoelectric effect which involves the absorption of a photon with subsequent ejection of an atomic electron. Compton scattering predominates in the middle energy range of 0.5 to 1.0 MeV. In this process, an elastic collision occurs between a photon and a single electron which results in the transfer of

energy from the former to the latter with the subsequent deflection of the photon path and the ejection of the electron from the atom. Electron pair formation involves the absorption and pairing of an incoming photon with an electron and giving it sufficient kinetic energy to escape from the atom. A minimum of 1.02 MeV (Kohl et al., 1961) is needed for the phenomena to occur. The mechanism of electron pair production can be considered to be negligible in soil-water analysis since water is a poor absorber of high energy gamma-rays (Ferguson and Gardner, 1962). As a consequence, radioactive sources used in water content measurements are limited to those emitting primary radiation in the middle or lower energy range. Cesium-137 satisfies this condition having its primary energy peak at 0.663 MeV. In this middle energy range, Compton scattering is the most important of the three processes (Gurr, 1962).

Van Bavel et al. (1957) emphasized that the attenuation equation cannot be used to calculate water content in soils unless all scattered and secondary radiation had been discriminated against through pulse height analysis. On the other hand, Saxena et al. (1970) suggested that pulse height analysis was not required if long narrow slits were used to collimate the gamma-ray beam. For precise water content measurements, however, pulse height analysis is desirable. A method described by Fritton (1969) can also be used to correct gamma-ray attenuation measurements for the combined effects of resolving time (the minimum time that the detector can separate two consecutive photons), gamma-ray scattering and absorption processes.

## MATERIALS AND METHODS

### Soil

The soil used in this study was the Molokai soil which is classified as a Typic Torrox under the Order Oxisols by the United States Comprehensive Soil Classification System.

### Instrumentation

The source of gamma radiation was cesium-137<sup>1</sup> which had a strength of 220 millicuries. Selection of cesium-137 was based primarily on its readily availability, long half-life (33 years) and monoenergetic peak at 0.663 MeV. The cesium-137 source, sealed in a stainless steel capsule, was placed in the center of a cylindrical lead container, 16 cm in diameter and 16 cm in height. A rectangular slit, 2 cm in width and 1 mm in height, was cut to the center of the lead container. This allowed emission of a collimated beam of gamma radiation to be transmitted to a NaI (TI) scintillation detector<sup>2</sup>. The crystal face of the detector was covered by a 4 cm thick lead collimator with a rectangular slit measuring 3 cm in width and 1 mm in height. This collimator minimized scattered radiation from reaching the detector.

Both detector and source housing could be manually adjusted until the collimated gamma-ray beam was aligned. Perfect collimation was reflected by the maximum counting rate recorded by a ratemeter<sup>3</sup> and

---

<sup>1</sup>Nuclear-Chicago Corporation, 1611 Beverly Boulevard, Los Angeles, California.

<sup>2</sup>Ibid, Model 956.

<sup>3</sup>Ibid, Model 9733.

scalar<sup>4</sup> via a pulse height analyzer<sup>5</sup>. With the pulse-height analyzer set at the wide differential counting mode and a 1-volt window, the emitted gamma radiation lacked the necessary intensity to yield adequate count rates for small counting times. Hence, the pulse-height analyzer was switched to integral mode and set to discriminate against photons of energy of less than 0.550 MeV. Collimation of gamma-rays permitted analysis of soil thickness nearly equivalent to that of the detector slit width.

Detector and source housing were secured on a horizontal platform and were driven in either vertical direction by a 1/4 HP motor connected to a vertically positioned threaded rod (Figure 22). A double throw electrical switch controlled the positioning of both source and detector along the length of a stationary soil column. "Standard" counting measurements were made through a permanently positioned aluminum absorber, 8.89 cm in diameter. These measurements were frequently repeated in order to check for any changes in the counting rate due to instrumentation or alignment of the collimated beam and to radioactive decay. The absorber also served as the holder for the vertically positioned soil column

#### Correction Factor for Variation in Standard Counts

The standard count is that scalar reading (count/time) obtained after the collimated gamma-ray beam passes through the standard absorber

---

<sup>4</sup>Ibid, Model 812830.

<sup>5</sup>Ibid, Model 8725.

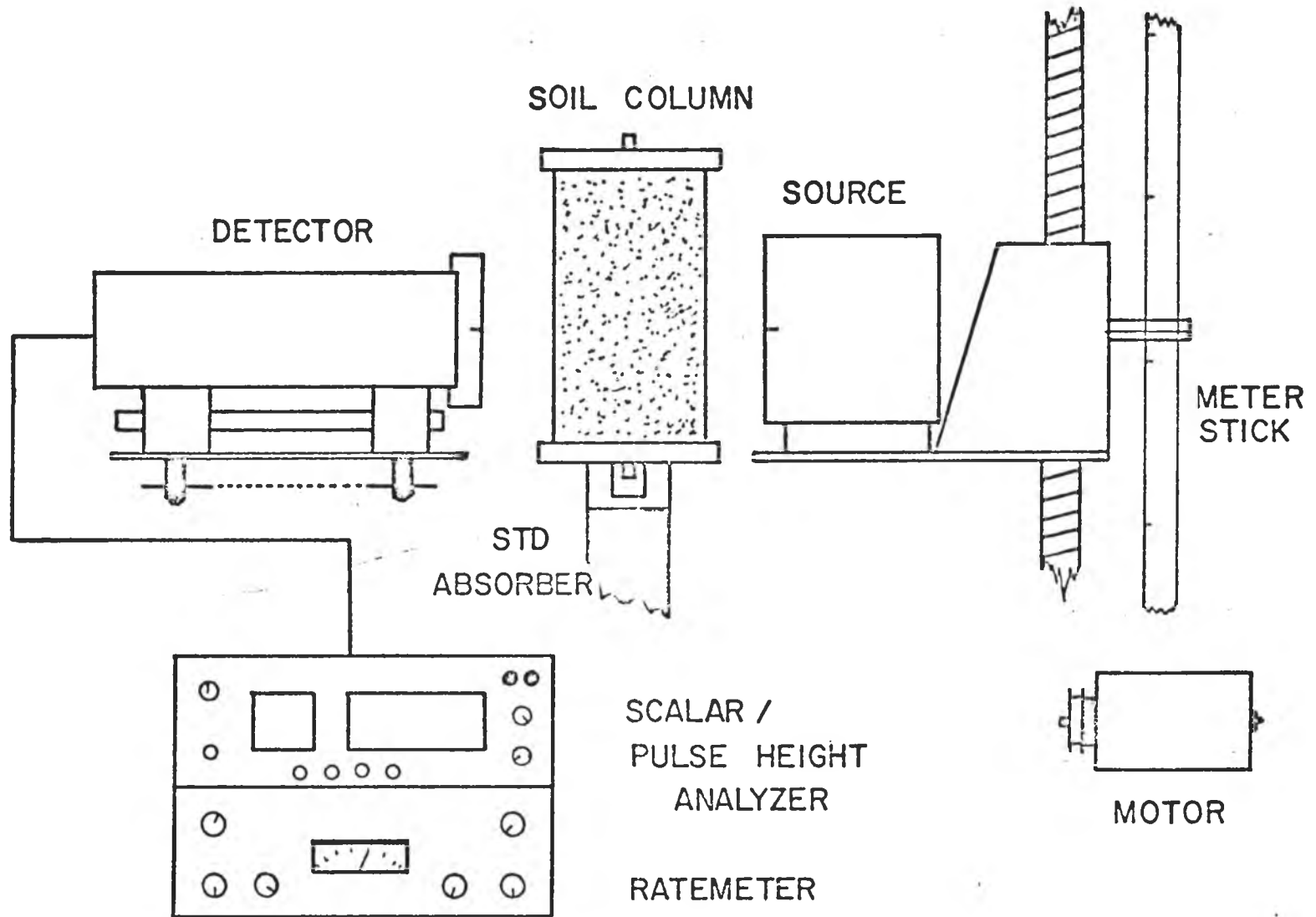


Figure 22. Diagram of Gamma-ray Assembly and Instrumentation.

(permanent aluminum base). Over short time intervals, the detection and counting equipments are relatively stable. However, significant differences between standard count measurements may be observed because of daily instrumental variations and radioactive decay of the source. A correction factor is required to scale the gamma-ray data of one day to that of another for comparison purposes. The correction factor may be expressed as

$$CF = N_{1std}/N_{2std}$$

where  $N_{1std}$  and  $N_{2std}$  are standard counts obtained at different times. The scaled data reading,  $N_{corrected}$ , is

$$N_{corrected} = N_{observed}/CF.$$

#### Counting Precision

The standard deviation  $\sigma$  of a counting rate from a random emitting radioactive source is approximately

$$\sigma = (N/t)^{1/2}$$

where  $t$  is the counting time and  $N$  the radiation count. For our soil,  $N/t$  was approximately 160,000 counts/minute and one standard deviation was equivalent to 400 counts/minute.

Instrumentation errors depends upon the characteristics of the particular equipment. The error is generally small, however, it is common practice to multiply the standard deviation by a factor of 1.5 to 2 to account for instrument error.

Calibration-curve errors must be considered subjectively since they depend upon the care taken in the calibration process and the degree to which experimental conditions are comparable to calibration conditions. The common practice is to regard such errors as negligible as compared

to those arising from experimental variability.

#### Resolving Time Correction

The combined effects of scattering, absorption and resolving time tend to lower the overall accuracy of the system. Fritton (1969) described a method in which the observed results could be corrected for the aforementioned effects. The observed counting rate  $N$  (cpm) was corrected by using

$$R = N/[1 - (T)(N)]$$

where  $R$  is the true counting rate (cpm) and  $T$  the resolving time (min/count).  $T$  is an experimentally determined constant which minimizes the deviation from linear regression for data of  $\ln(N)$  versus  $x$  (thickness).

Fritton experimentally found the resolving times for soil and water to be almost identical, therefore, he was able to use a single  $T$  for his soil-water system. For our soil-water system, the resolving time was determined and compared using air-dried soil and distilled water.

#### Verification of Attenuation Equation

Water, Molokai soil and a mixture of both were used to test the validity of the attenuation equation for our experimental conditions. This procedure essentially involved the test of proportionality between the semi-logarithm of gamma-ray intensity ratio and the variables  $\rho$  and  $x$  in the quantity  $\rho\mu x$ .

To test the attenuation equation for our experimental system and to determine the mass attenuation coefficient of water, a cylindrical plexiglas container with equally spaced partitioned compartments was used. The thickness of water was successively increased by filling the compartments after each measurement.  $N_c$  was taken as the initial

intensity reading through the empty container. Verification of equation (11a) for water would also permit the mass attenuation coefficient of water to be computed from the slope of  $\ln(N_C/N_W)$  and  $x$  plot.

For the Molokai soil, it was easier to pack a cylindrical plexiglas varying the thickness of the sample. In accord with equation (6a), values of  $\ln(N_C/N_d)$  were plotted against corresponding values of bulk densities in order to verify the proportional relationship between them. The final test was to establish the accuracy of the instrumentation in measuring soil-water content. This was accomplished by using the gamma-ray data to calculate the water content from equation (12a) and then sectioning and gravimetrically determining the water content at each analyzed position of the soil column.

## RESULTS AND DISCUSSION

Use of equation (2a) to measure soil density and water content is only valid if an exponential or a linear semi-logarithmic relationship can be shown to exist between the ratio of photon count ( $N_0/N$ ) and  $\mu\rho x$ .

### Counting Precision and Resolving Time

The counts/minute variation was approximately  $2\sigma$  or 800 counts/minute for a gamma-ray scan at a given position.

Resolving times for both soil and water were determined to be 4.9 microseconds.

### Attenuation Coefficient for Water

When water alone was the attenuating material, a linear semi-logarithmic relationship between  $\ln(N_C/N_W)$  and  $x_W$  with intercept of -0.00252 was obtained (Figure 23). With a water density of  $0.9978 \text{ g/cm}^3$  at  $22^\circ \text{ C}$ , the mass attenuation coefficient of water from the slope of the computed regression line with no resolving time correction was  $0.08062 \text{ cm}^2/\text{g}$ . Davidson et al. (1963) and Kirkham et al. (1967) reported uncorrected values of 0.0815 and  $0.0802 \text{ cm}^2/\text{g}$ , respectively. Using Fritton's (1969) correction method, a resolving time correction of 4.9 microseconds was obtained. With resolving time correction of 9 and 5 microseconds, Gurr (1962) and Fritton (1969) obtained mass attenuation coefficients of water of 0.0856 and  $0.0867 \text{ cm}^2/\text{g}$ , respectively. Grodstein (1957) reported a theoretical value for water of  $0.0857 \text{ cm}^2/\text{g}$ .

### Attenuation Coefficient for Molokai Soil

Air-dried Molokai soil of less than 2 mm size was the second material used in testing equation (2a). A cylindrical plexiglas

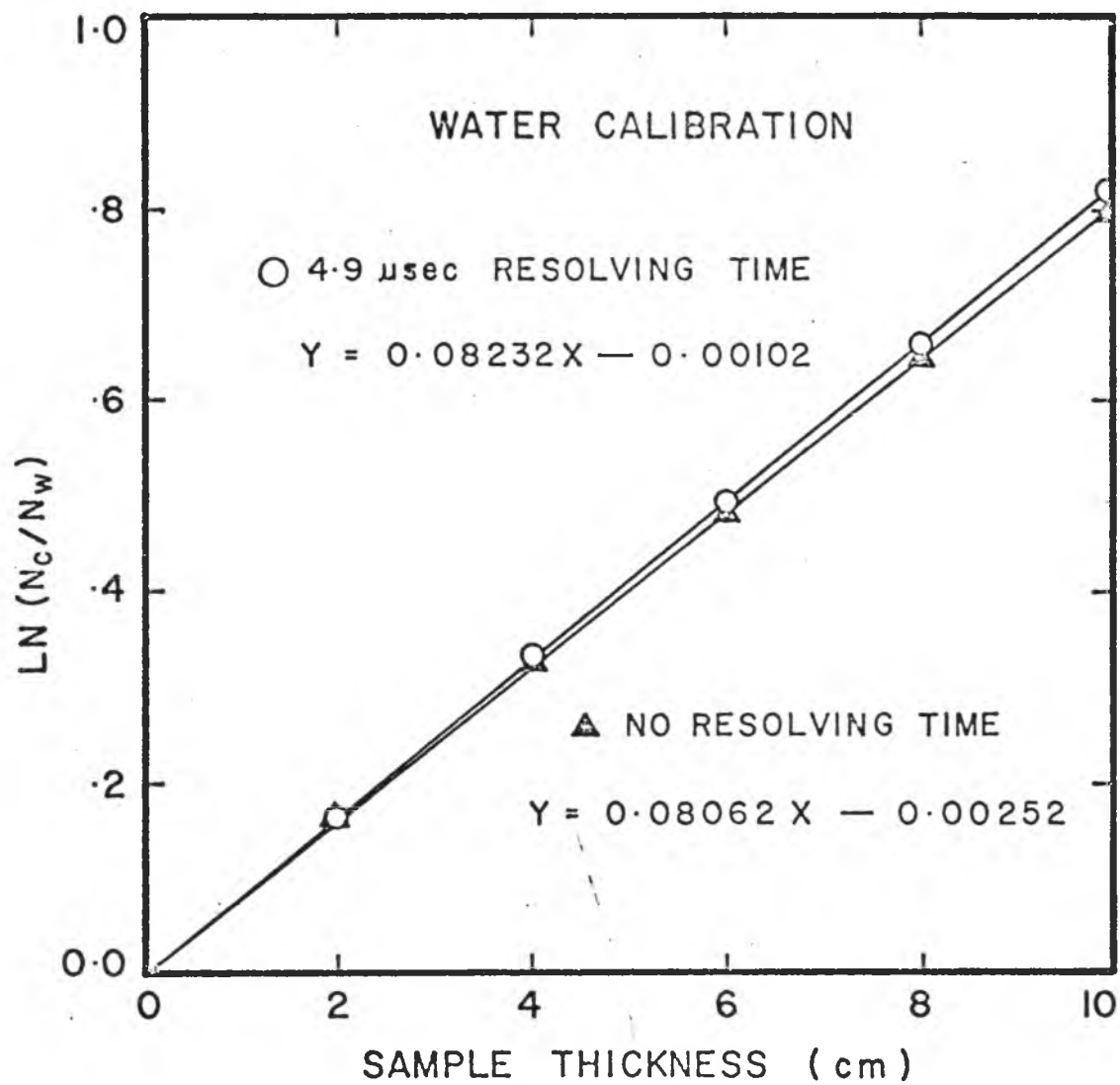


Figure 23. Experimental Verification of the Gamma-ray Attenuation Equation, with Water Thickness  $x$  as the Independent Variable.

container, 5 cm in height and 8.19 cm in diameter, was packed with soil to different bulk densities. Gamma-ray measurements were taken at positions 0.5 cm apart on the column. The mean  $\ln(N_C/N_D)$  for each packing was plotted against the respective mean bulk density (Figure 24), and the correlation was found to be significantly linear for the uncorrected and corrected plots. Based on equation (8), the mass attenuation coefficient for the Molokai soil could then be calculated by dividing the slope of the regression line by the soil thickness (8.19 cm). Average uncorrected and corrected values of 0.07619 and 0.07785  $\text{cm}^2/\text{g}$  were obtained. Mass attenuation coefficients of 0.07785  $\text{cm}^2/\text{g}$  (Reginato and van Bavel, 1964), 0.0710  $\text{cm}^2/\text{g}$  (Shalhevet and Yaron, 1964) and 0.0689  $\text{cm}^2/\text{g}$  (Kirkham et al., 1967) have been reported. The latter two values were uncorrected for resolving time. The disparity of values reported was probably due to the different mineral composition of the soils used.

#### Comparison of Water Content Measurements

Based on the experimental mass attenuation coefficients for water and soil, the volumetric water content can be calculated by using equation (12a). A 20 cm long plexiglas column with a 8.19 cm diameter was packed with soil to a uniform density and partially saturated with water by capillarity for 48 hours. The volumetric water content at positions along the length of the column was calculated from gamma-ray attenuation data. The column was then sectioned and oven-dried. The results for both determinations were tabulated in Table 2. A mean difference of 0.0078 cc/cc was found between water contents determined from gravimetric and gamma-ray measurements when the resolving time correction of 4.9 microseconds was used on the latter. A larger difference was noted if

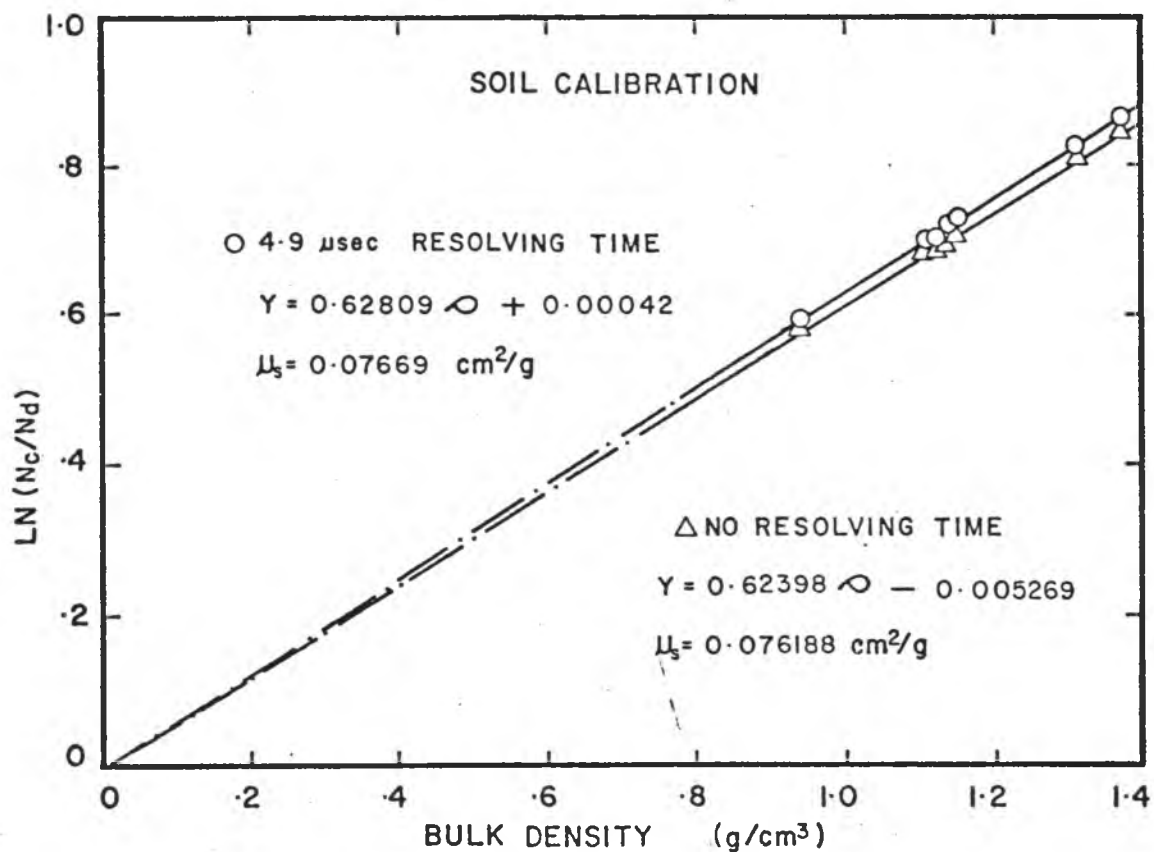


Figure 24. Experimental Verification of the Gamma-ray Attenuation Equation for Molokai Soil, with Mean Bulk Density,  $\rho$ , as the Independent Variable.

TABLE 2. -- Bulk Density and Water Content measurements for Molokai soil with and without resolving time correction (T,  $\mu\text{sec}$ ).

Position (cm)	Bulk Density (g/cm <sup>3</sup> )	(Volumetric Water Content (cm <sup>3</sup> /cm <sup>3</sup> ))		
		T=0	T=4.9	
5	1.2276	.5134	.5184	.5184
6	1.2431	.5149	.5154	.5188
7	1.2399	.5113	.5161	.5195
8	1.2509	.5161	.5146	.5180
9	1.2543	.5220	.5137	.5170
10	1.2573	.5170	.5133	.5166
11	1.2614	.5154	.5083	.5115
12	1.2538	.5095	.5085	.5091
13	1.2536	.5112	.5106	.5139
14	1.2518	.5194	.5066	.5099
15	1.2485	.5178	.5031	.5065
16	1.2360	.5098	.5101	.5135
17	1.2301	.5039	.5070	.5105
Mean	1.2468	.5140*	.5112**	.5144**
Stand. Dev.	0.0106	.0048	.0044	.0046
Difference			.00545	.00078

\*Volumetric water content obtained by sectioning of soil column.

\*\*Volumetric water content determined by gamma-ray attenuation.

no resolving time correction was used. Discrepancies between water contents at different positions were attributed to methodology. The gamma-ray beam scanned a 1 mm section, whereas, gravimetric determinations were made on 1 cm thick sections.

## CONCLUSIONS

The gamma-ray attenuation technique is another valuable tool in soil-water studies. Rapid and non-destructive bulk density and water content measurements can be made with a high degree of accuracy once instrument calibration and verification of the attenuation equation for the experimental system are complete. Use of experimentally determined mass attenuation coefficients rather than the theoretical values of the attenuating mass was desirable for precise measurement of water content and density.

Limitations of the system could be enumerated as follows: (1) it is valid only for non-expanding porous media, (2) equipment is costly, and (3) considerable shielding is required for a 220 millicurie cesium-137 source. Americium-241 may be a more suitable source for field work since it requires less shielding.

## LITERATURE CITED

1. Bernhard, R. K., and M. Chasek. 1955. Soil density determination by direct transmission of gamma rays. A.S.T.M., Philadelphia, Pa. Preprint No. 86.
2. Davidson, J. M., D. R. Nielsen, and J. W. Biggar. 1963. Gamma-radiation attenuation for measuring density and transient water flow in porous media. *J. Geophys. Res.* 68(16):4777-4783.
3. Ferguson, H., and W. H. Gardner. 1962. Water content measurement in soil column by gamma ray absorption. *Soil Sci. Soc. Amer. Proc.* 26:11-14.
4. Ferguson, H., and W. H. Gardner. 1963. Diffusion theory applied to water flow data obtained using gamma ray absorption. *Soil Sci. Soc. Amer. Proc.* 27(3):243-246.
5. Fritton, D. D. 1969. Resolving time, mass absorption coefficient and water content with gamma-ray attenuation. *Soil Sci. Soc. Amer. Proc.* 33:651-655.
6. Grodstein, G. W. 1957. X-ray attenuation coefficients from 100 KeV to 100 MeV. NBS U.S. Circular 583.
7. Gurr, C. G. 1962. Use of gamma-rays in measuring water content and permeability in unsaturated columns of soil. *Soil Sci.* 94: 224-229.
8. Hayward, E., and J. H. Hubbel. 1953. An experiment on gamma ray back scattering. Nat. Bur. of Stand., Washington, D. C. Rep. No. 2264.
9. King, L. G. 1967. Gamma-ray attenuation for soil-water-content measurements using americium-241. Proc. Series, IAEA and FAO, Vienna. pp. 17-29.
10. Kirkham, D., D. E. Rolston, and D. D. Fritton. 1967. Gamma-radiation detection of water content in two-dimensional evaporation prevention experiments. Proc. Series, IAEA and FAO, Vienna. pp. 3-16.
11. Kohl, J., R. D. Zentner and H. R. Lukeus. 1961. Radioisotope Application Engineering. D. Van Norstrand Co., New Jersey, pp. 305-321.
12. Reginato, R. J., and C. H. M. van Bavel. 1964. Soil water measurement with gamma attenuation. *Soil Sci. Soc. Amer. Proc.* 28(6): 721-724.

13. Saxena, G. S., R. E. Franklin, and G. S. Taylor. 1970. Importance of pulse-height analysis in the gamma-ray attenuation technique for measurement of soil moisture. *Soil Sci.* 110(4): 283-286.
14. Shalhevet, J., and B. Yaron. 1967. Ion distribution, moisture content and density of soil column measured with gamma radiation. *Soil Sci. Soc. Amer. Proc.* 31(2):153-156.
15. Van Bavel, C. H. M., N. Underwood, and S. R. Ragar. 1957. Transmission of gamma rays by soil and soil densitometry. *Soil Sci. Soc. Amer. Proc.* 21:588-599.
16. Vomocil, J. A. 1954. In situ measurement of soil bulk density. *Agri. Eng.* 35:651-654.
17. Whisler, F. D., A. Klute, and D. B. Peters. 1968. Soil water diffusivity from horizontal infiltration. *Soil Sci. Soc. Amer. Proc.* 32:6-11.

APPENDIX B

TABULATION OF EXPERIMENTAL HYSTERESIS DATA

TABLE 3. -- Tabulation of Molokai Soil Experimental Hysteresis Data\*

Molokai Soil

-Pressure Head (cm)	Vol. Water Content (cc/cc)	-Dimen. Press. Head (cm/cm)	Deg. of Sat. (cc/cc)
------------------------	-------------------------------	--------------------------------	-------------------------

---

## Initial Desorption Scan

0.0	.5049	0.000	.8824
39.1	.5084	1.801	.8885
61.0	.5067	2.809	.8885
80.0	.5083	3.687	.8884
93.3	.5053	4.300	.8830
107.3	.5003	4.947	.8744
120.0	.4989	5.530	.8720
132.5	.4867	6.106	.8506
150.3	.4555	6.926	.7961
176.2	.4428	8.120	.7738
199.3	.4354	9.186	.7610

## Main Absorption Scan

199.3	.4354	9.186	.7610
169.8	.4398	7.827	.7686
153.3	.4411	7.065	.7709
137.2	.4534	6.324	.7924
117.1	.4586	5.398	.8014
103.5	.4695	4.768	.8205
76.8	.4828	3.538	.8438
62.5	.4898	2.880	.8560
42.5	.4958	1.959	.8664
11.5	.5025	0.532	.8781
4.6	.5020	0.211	.8774
0.0	.5016	0.000	.8766

## Main Desorption Scan

0.0	.5016	0.000	.8766
40.0	.5022	1.843	.8777
81.3	.4998	3.747	.8734
104.6	.4959	4.820	.8667
131.8	.4675	6.074	.8170
149.8	.4539	6.903	.7933
176.2	.4428	8.120	.7740
199.2	.4354	9.200	.7610

TABLE 3, CONTINUED

## Absorption Scan 1

149.8	.4539	6.903	.7933
134.6	.4572	6.203	.7990
120.2	.4666	5.539	.8155
.02.3	.4699	4.714	.8211
83.1	.4831	3.829	.8443
64.2	.4925	2.959	.8606
41.5	.4991	1.912	.8723
20.9	.4984	0.963	.8711
2.4	.4979	0.111	.8702
0.0	.4988	0.000	.8717

## Absorption Scan 2

130.5	.4682	6.014	.8183
114.5	.4776	5.276	.8347
94.5	.4826	4.355	.8434
71.9	.4893	3.313	.8552
53.0	.4982	2.441	.8707
30.4	.4980	1.402	.8703
11.5	.5002	0.528	.8742
0.0	.5002	0.000	.8742

## Desorption Scan 1

59.5	.4960	2.742	.8669
80.8	.4919	3.724	.8597
113.1	.4892	5.212	.8550
132.5	.4690	6.106	.8195
149.8	.4623	6.903	.8079
157.7	.4451	8.097	.7738

## Desorption Scan 2

89.9	.4828	4.143	.8437
108.4	.4757	4.995	.8313
126.0	.4679	5.806	.8177
143.3	.4574	6.604	.7994
158.5	.4471	7.304	.7813

---

\*data at column position L=9 cm.

TABLE 4. -- Tabulation of Wahiawa Soil Experimental Hysteresis Data\*

-Pressure Head (cm)	Vol. Water Content (cc/cc)	-Dimen. Press. Head (cm/cm)	Deg. of Sat. (cc/cc)
------------------------	-------------------------------	--------------------------------	-------------------------

---

## Initial Desorption Scan

0.0	.5825	0.000	.8691
20.9	.5636	0.972	.8409
54.7	.5299	2.543	.7906
76.0	.4996	3.537	.7455
86.2	.4860	4.009	.7251
120.6	.4498	5.609	.6712
137.7	.4455	6.405	.6647
154.6	.4386	7.191	.6545
171.7	.4367	7.986	.6516

## Main Absorption Scan

171.7	.4367	7.986	.6516
151.8	.4389	7.060	.6549
132.7	.4327	6.172	.6456
106.1	.4458	4.935	.6651
82.6	.4607	3.842	.6874
52.4	.4882	2.437	.7285
18.8	.5192	0.877	.7751
0.0	.5774	0.000	.8615

## Main Desorption Scan

0.0	.5774	0.000	.8615
25.9	.5604	1.206	.8362
62.8	.5166	2.921	.7709
91.4	.4774	4.251	.7124
112.7	.4595	5.242	.6856
143.2	.4440	6.660	.6625
171.6	.4356	7.980	.6500

TABLE 4, CONTINUED

## Absorption Scan 1

76.5	.4965	3.558	.7408
54.2	.5132	2.521	.7657
29.7	.5327	1.381	.7948
9.3	.5577	0.433	.8322
0.0	.5737	0.000	.8560

## Absorption Scan 2

118.8	.4534	5.526	.6766
93.6	.4630	4.353	.6909
63.1	.4801	2.937	.7163
25.1	.5250	1.169	.7834
0.0	.5764	0.000	.8600

## Desorption Scan 1

10.2	.5463	0.475	.8151
28.1	.5366	1.346	.8007
52.5	.5115	2.442	.7632
84.1	.4859	3.910	.7250

## Desorption Scan 2

36.4	.5122	1.693	.7642
66.3	.4943	3.083	.7375
91.5	.4725	4.254	.7050
122.9	.4557	5.717	.6800
160.7	.4424	7.473	.6601

---

\*data at column position L=10 cm.

APPENDIX C  
CURVE FITTING PARAMETERS

TABLE 5. -- Curve Fitting Parameters

Molokai Soil

	$\theta_0$	$\theta_r$	$\phi_0$	$\beta$	$\epsilon$
Absorption Scans					
main	.8750	.7625	-5.307	-1.802	0.0
scan 1	.8750	.7950	-4.736	-1.949	0.0
scan 2	.8750	.8188	-4.479	-2.098	0.0
Desorption Scans					
main	.8750	.7625	-6.620	-3.740	0.0
scan 1	.8650	.7625	-6.727	-3.634	0.0
scan 2	.8444	.7625	-6.917	-3.112	0.0

Wahiawa Soil

	$\theta_0$	$\theta_r$	$\phi_0$	$\beta$	$\epsilon$
Absorption Scans					
main	.7950	.6480	-3.128	-1.240	0.0
scan 1	.7975	.6760	-2.743	-1.321	0.0
scan 2	.8175	.7400	-2.201	-1.526	0.0
Desorption Scans					
main	.8390	.6480	-4.162	-1.416	0.0
scan 1	.8150	.6480	-4.322	-1.380	0.0
scan 2	.7650	.6480	-4.863	-1.731	0.0

TABLE 5, CONTINUED

Sandy Loam Soil (Topp, 1969)

	$\theta_0$	$\theta_r$	$\phi_0$	$\beta$	$\epsilon$
Absorption Scans					
main	.3775	.3510	-1.015	-0.920	0.0
scan 1	.3775	.3075	-1.702	-1.050	0.0
scan 2	.3775	.2670	-1.950	-1.166	0.0
scan 3	.3775	.2390	-2.027	-0.955	0.0
scan 4	.3775	.2070	-2.177	-0.894	0.0
scan 5	.3775	.1650	-2.188	-0.735	0.0
Desorption Scans					
main	.3800	.1650	-4.554	-2.121	0.0
scan 1	.3350	.1650	-4.567	-1.289	0.0
scan 2	.2800	.1650	-5.083	-1.348	0.0
scan 3	.2480	.1650	-5.592	-1.581	0.0
scan 4	.2000	.1650	-6.963	-2.836	0.0

APPENDIX D

PREDICTED CURVE FITTING PARAMETERS  
FROM FIGURES 19 AND 20

TABLE 6. -- Predicted Curve Fitting Parameters from Figures 19 and 20

Molokai Soil

	$\theta_0$	$\theta_r$	$\phi$ at $\theta_r$	$\beta$	$\phi_0$
Absorption Scans					
scan 1'	.8750	.8100	-6.375	-2.043	-4.567
scan 2'	.8750	.7800	-7.500	-1.870	-4.960
Desorption Scans					
scan 1'	.8700	.7625	-1.875	-3.680	-6.675
scan 2'	.8550	.7625	-3.000	-3.470	-6.780

APPENDIX E

FORTRAN IV PROGRAM TO CONVERT RAW GAMMA-RAY DATA TO  
WATER CONTENT, DEGREE OF SATURATION AND  
DIMENSIONLESS PRESSURE HEAD.

## APPENDIX E

C DEFINITION OF INPUT VARIABLES:  
 C BD = BULK DENSITY  
 C DRYSTD = DRY STANDARD  
 C THETAG = INITIAL GRAVIMETRIC WATER CONTENT  
 C TOP = MAXIMUM COLUMN POSITION  
 C AL = COLUMN LENGTH  
 C PORE = POROSITY  
 C N = NUMBER OF POSITIONS  
 C STD = STANDARD READING  
 C W TO W4 = SOIL TYPE AND HISTORY  
 C Z = DECISION VARIABLE. SATURATED--Z=0.0: UNSATURATED--Z=9.9  
 C HH = PRESSURE HEAD  
 C X = COLUMN POSITION  
 C DRY = DRY SOIL ATTENUATED INTENSITY ("WET" FOR WET SOIL)  
 C INTIAL = INITIAL VOLUMETRIC WATER CONTENT  
 C T = RESOLVING TIME  
 C ATTW = ATTENUATION COEFFICIENT OF WATER ("ATTS" FOR SOIL)  
 C TX = INSIDE DIAMETER OF SOIL COLUMN  
 DIMENSION ADRY(20),X(20),DRY(20),AWET(20),WET(20),THETA(20),  
 1 DTHETA(20),HEAD(20),DHEAD(20),T3(100),T5(100),T6(100),  
 2 T7(100),T8(100),T9(100),S3(100),S4(100),S5(100),S6(100),  
 3 S7(100),S8(100),S9(100)  
 REAL INTIAL  
 K=0

## APPENDIX E, CONTINUED

```
READ (5,1) BD, DRYSTD, THETAG, ATTS, TOP, AL, PORE
1  FORMAT(7F10.0)
   T=0.81667E-07
   ATTW=0.08232
   TX=8.19
   INTIAL=BD*THETAG
17  CONTINUE
   READ (5,2) N, STD
2   FORMAT(I3,7X,F10.2)
   EN=FLOAT(N)
C   N=99 IS THE CONDITION CODE TO START COMPILING POSITION DATA.
   IF (N.EQ.99) GO TO 18
   READ(5,3) W, W1, W2, W3, W4
3   FORMAT(5A4)
   READ(5,4) Z, HH
4   FORMAT(F10.0/10.0)
   XX=HH + TOP
   CR=DRYSTD/STD
   A=ATTW*TX
   SUM=0.0
   SSUM=0.0
   IF (K.GT.0) GO TO 100
   DO 6 I=1,N
   READ(5,5) X(I), ADRY(I)
5   FORMAT(2F10.0)
```

## APPENDIX E, CONTINUED

```
C   CORRECTION FOR RESOLVING TIME
6   DRY(I)=ADRY(I)/(1.0 - (T*ADRY(I)))
100 CONTINUE
    DO 9 I=1,N
    READ (5,7) AWET(I)
7   FORMAT (10X,F10.0)
    WET(I)=AWET(I)/(1.0 - (T*AWET(I)))
    B=ALOG(DRY(I)/WET(I)*CR)
    THETA(I)=B/A + INTIAL
C   THETA = CALCULATED WATER CONTENT
    DTHETA(I)=THETA(I)/PORE
C   DTHETA = DIMENSIONLESS WATER CONTENT
C   IF Z EQUAL ZERO THEN CALCULATED STANDARD DEVIATION AMONG POSITIONS.
    IF (Z.EQ.9.9) GO TO 8
    SUM=SUM + THETA(I)
    SSUM=SSUM + THETA(I)**2
8   CONTINUE
    HEAD(I)=XX - X(I)
    DHEAD(I)=HEAD(I)/AL
C   HEAD = PRESSURE HEAD; DHEAD = DIMENSIONLESS PRESSURE HEAD.
    IF (HEAD(I).GT.0.0) GO TO 9
    HEAD(I)=0.0
9   CONTINUE
    IF (Z.EQ.9.9) GO TO 10
    SS=SSUM - SUM**2/EN
```

## APPENDIX E, CONTINUED

```

ST=SQRT(SS/(EN - 1.0))
STDE=ST/(SQRT(EN))
10  AVER=SUM/EN
C   OUTPUT SECTION OF THE PROGRAM.
    WRITE (6,11) W, W1, W2, W3, W4, HH
11  FORMAT ('1'.10X,'CALCULATIONS OF THETA',5X,5A4,5X,'HEAD AT TOP
1    OF COLUMN =' ,F6.2///T6,'POSITION',T21,'HEAD',T28,'THETA',
2    T42,'DRY',T56,'WET',T70,'ORIGINAL READINGS',T91,'HEAD',T100,
3    'DTHETA',T109,'POSITION')
    DO 13 I=1,N
    WRITE (6,12) X(I), HEAD(I), THETA(I), DRY(I), WET(I), ADRY(I),
1    AWET(I), DHEAD(I), DTHETA(I), X(I)
12  FORMAT (T3,F10.1,T18,F7.2,T28,F6.4,T38,F10.2,T51,F10.2,T64,
1    F10.2,T77,F10.2,T91,F6.2,T100,F6.4,T109,F6.1)
13  CONTINUE
    IF (Z.EQ.9.9) GO TO 15
    WRITE (6,14) ST, STDE, AVER
14  FORMAT (///' ',20X,'STANDARD DEV. =' ,F10.4,10X,'STANDARD ERROR =' ,
1    F10.4///20X,'AVERAGE THETA VALUE =' ,F10.4)
15  CONTINUE
16  FORMAT (///21X,'INPUT CONSTANTS'//15X,'ATTW =' ,F6.4/15X,'ATTS =' ,
1    F6.4/15X,'SAMPLE LENGTH =' ,F5.3/15X,'STD OF WET SOIL =' ,F10.2/
2    15X,'STD OF DRY SOIL =' ,F10.2/15X,'N =' ,I3/15X,'INITIAL
3    GRAVIMETRIC WATER CONTENT =' ,F6.4/15X,'POROSITY =' ,F6.4)
    WRITE (6,16) ATTW, ATTS, TX, STD, DRYSTD, N, THETAG, PORE

```

## APPENDIX E, CONTINUED

```
C THIS PORTION OF THE PROGRAM SEPARATE DTHETA WRT DHEAD FOR 7
C DIFFERENT COLUMN POSITIONS.
K=1 + K
T3(K)=DTHETA(3)
T4(K)=DTHETA(4)
T5(K)=DTHETA(5)
T6(K)=DTHETA(6)
T7(K)=DTHETA(7)
T8(K)=DTHETA(8)
T9(K)=DTHETA(9)
S3(K)=DHEAD(3)
S4(K)=DHEAD(4)
S5(K)=DHEAD(5)
S6(K)=DHEAD(6)
S7(K)=DHEAD(7)
S8(K)=DHEAD(8)
S9(K)=DHEAD(9)
GO TO 17
18 CONTINUE
WRITE (6,19) X(3)
19 FORMAT ('1',20X,'DIMENSIONLESS HEAD VS DEGREE OF SATURATION//
1 ' POSITION',F5.1///' ',T10,'HEAD',T30,'THETA')
DO 21 I=1,N
WRITE (6,22) S3(I), T3(I)
22 FORMAT (' ',T5,F10.3,T30,F7.4)
```

## APPENDIX E, CONTINUED

```
21  CONTINUE
    WRITE (6,19) X(4)
    DO 23 I=1,K
    WRITE (6,22) S4(I), T4(I)
23  CONTINUE
    WRITE (6,19) X(5)
    DO 24 I=1,K
    WRITE (6,19) S5(I), T5(I)
24  CONTINUE
    WRITE (6,22) X(6)
    DO 25 I=1,K
    WRITE (6,22) S6(I), T6(I)
25  CONTINUE
    WRITE (6,19) X(7)
    DO 26 I=1,K
    WRITE (6,22) S7(I), T7(I)
26  CONTINUE
    WRITE (6,19) X(8)
    DO 27 I=1,K
    WRITE (6,22) S8(I), T8(I)
27  CONTINUE
    WRITE (6,19) X(9)
    DO 28 I=1,K
    WRITE (6,22) S9(I), T9(I)
28  CONTINUE
    STOP
```

## APPENDIX E, CONTINUED

END

APPENDIX F

FORTRAN IV PROGRAM TO CALCULATE THE  
CURVE FITTING PARAMETERS.

## APPENDIX F

DIMENSION THETA(50), PHI(50), THETAC(50)

C DEFINITION OF VARIABLES:

C THETA IS THE EXPERIMENTAL WATER CONTENT

C THETAC IS THE CALCULATED WATER CONTENT

C E, PHIO, BETA ARE CURVE FITTING PARAMETERS

C PHI IS THE PRESSURE HEAD READ IN AS A POSITIVE VALUE

C THETAO AND THETAR ARE END POINTS OF THE SCANNING CURVE

C (WATER CONTENT VALUES)

17 CONTINUE

READ (5,2) N1, A

C A\*N1 IS THE LOWER BOUND OF E AND A\*KA THE UPPER BOUND

C END OF DATA SET WHEN READ 99 CARD

IF (A.GT.100) GO TO 16

READ (5,2) N3, C

C B\*N2 IS THE LOWER BOUND OF PHIO AND B\*KB THE UPPER BOUND

READ (5,2) N3, C

C C\*N3 IS THE LOWER BOUND OF BETA AND C\*KC THE UPPER BOUND

2 FORMAT (I10,2F10.0)

READ (5,25) KA, KB, KC

25 FORMAT (3I10)

C XYZ IS THE LENGTH OF THE COLUMN. IF THE PRESSURE HEAD IS READ

C IN AS THE DIMENSIONLESS FORM THEN LET XYZ = 0.0

READ (5,30) XYZ

30 FORMAT (F10.0)

READ (5,555) N, THETAO, THETAR

## APPENDIX F, CONTINUED

```

C      N IS THE NUMBER OF THETA OR PHI VALUES
5555  FORMAT (I3,7X,2F10.0)
      READ (5,3) (THETA(I), I=1,N)
      READ (5,3) (PHI(I), I=1,N)
      DO 5I=1,N
      IF (XYZ.EQ.0.0) GO TO 55
      PHI(I)=-PHI(I)/XYZ
C      CHANGING PHI TO NEGATIVE VALUES AND TO THE DIMENSIONLESS FORM
      GO TO 5
55    PHI(I)=-PHI(I)
5     CONTINUE
3     FORMAT (8F10.0)
      WRITE (6,21)
21    FORMAT ('1',///' LEAST SQUARE',13X,'E',18X,'PHIO',18X,'BETA'///)
C      CALCULATION OF GAMMA
      GAMMA=(THETA0-THETAR)/(THETA0+THETAR)
C      COMBINATION OF E, PHIO AND BETA FITTING PARAMETERS
      SSUM2=0.0
      DO 50 I=KA,N1
C      N1=NO. OF E COUNTS
      JJ=I-1
      E=FLOAT(JJ)
      COSHE=0.5*(EXP(E)+EXP(-E))
      CONST=COSHE*GAMMA
      DO 40 I2=KB,N2

```

## APPENDIX F, CONTINUED

```
C   N2=NO. OF PHIO COUNTS
    PHIO=B*FLOAT(I2)
    DO 10 I3=KC,N3
C   N3=NO. OF BETA COUNTS
    BETA=C*FLOAT(I3)
C   CALCULATION OF THETAC WITH INPUT AND FITTING PARAMETERS
    SSUM=0.0
    DO 14 K=1,N
C   N=NO. OF PHI AND THETA DATA
    IF (PHI(K).GE.0.0) GO TO 11
C   PHI IS NEGATIVE AND DIVISION BY ZERO IS UNDEFINED
    XPHI=PHI(K)/PHIO
    X=XPHI**BETA+E
    IF (X.GT.174.0) GO TO 10
    COSHX=0.5*(EXP(X)+EXP(-X))
C   CALCULATED VALUES OF THETA...THETAC
    THETAC(K)=THETA0*(COSHX-CONST)/(COSHX+CONST)
    GO TO 12
11  THETAC(K)=THETA0
C   SOLVING FOR BEST FIT CURVE USING LEAST SQUARES METHOD
12  DIFF=THETA(K)-THETAC(K)
    SQUARE=DIFF**2
14  SSUM=SSUM+SQUARE
    IF (SSUM2.LT.SSUM) GO TO 15
    WRITE (6,1) SSUM, E, PHIO, BETA
```

## APPENDIX F, CONTINUED

```
1   FORMAT (1X,E16.8,3F15.4)
    GO TO 20
15  WRITE (6,4) SSUM, E, PHIO, BETA
4   FORMAT (1X,E16.8,3F15.4,'@@@@')
20  CONTINUE
    SSUM2=SSUM
10  CONTINUE
40  CONTINUE
50  CONTINUE
    GO TO 17
16  CONTINUE
    STOP
    END
```